Title: A Massively Parallel CRISPR-Based Screening Platform for Modifiers of Neuronal Activity

Authors: Steven C. Boggess[1,2], Vaidehi Gandhi[1,2], Ming-Chi Tsai[4], Emily Marzette[,2], Noam Teyssier[1,2,5], Joanna Yu-Ying Chou[1,2,3], Xiaoyu Hu[6], Amber Cramer[4], Lin Yadanar[1,2], Kunal Shroff[1,2,7,8], Claire G Jeong[4], Celine Eidenschenk[6], Jesse E. Hanson[4], Ruilin Tian[1,2], Martin Kampmann[1,2,9,10].

1. Institute for Neurodegenerative Diseases, University of California, San Francisco, San Francisco, CA, USA
2. Weill Institute for Neurosciences, University of California, San Francisco, San Francisco, CA, USA
3. City College of San Francisco, San Francisco, CA, USA.
4. Department of Neuroscience, Genentech, South San Francisco, CA, USA
5. Biological and Medical Informatics Graduate Program, University of California, San Francisco, San Francisco, CA, USA
6. Department of Functional Genomics, Genentech, South San Francisco, CA, USA
7. Neuroscience Graduate Program, University of California, San Francisco, San Francisco, CA, USA
8. Medical Scientist Training Program, University of California, San Francisco, San Francisco, CA, USA
9. Department of Biochemistry and Biophysics, University of California, San Francisco, San Francisco, CA, USA
10. Correspondence: martin.kampmann@ucsf.edu

Abstract:

Understanding the complex interplay between gene expression and neuronal activity is crucial for unraveling the molecular mechanisms underlying cognitive function and neurological disorders. Here, we developed pooled screens for neuronal activity, using CRISPR interference (CRISPRi) and the fluorescent calcium integrator CaMPARI2. Using this screening method, we evaluated 1343 genes for their effect on excitability in human iPSC-derived neurons, revealing potential links to neurodegenerative and neurodevelopmental disorders. These genes include known regulators of neuronal excitability, such as TARPs and ion channels, as well as genes associated with autism spectrum disorder and Alzheimer's disease not previously described to affect neuronal excitability. This CRISPRi-based screening platform offers a versatile tool to uncover molecular mechanisms controlling neuronal activity in health and disease.

Introduction

Billions of neurons in the human brain form a complex, dynamic network that gives rise to the emergent properties of cognition, memory, and behavior. Different neuronal cell types in the brain are defined by distinct patterns of gene expression,[1–4] with recent studies demonstrating these genetically defined subtypes can have distinguishable spike patterns.[5] Neuronal activity, in turn, further alters gene expression to affect the composition of synaptic receptors and ion channels at the neuronal membrane, making activity-dependent gene expression critical for long-lasting plasticity.[6,7] Large-scale efforts to map gene expression to different areas of the brain,[8,5] at single cell resolution[9,10], or to connect transcriptional changes to electrophysiological measurements[11] are underway, but we lack a systematic understanding of how expression differences of individual genes affect neuronal activity.

One approach to link genes to neuronal activity and brain function is to map genetic risk factors underlying neurological disorders that are characterized by neuronal activity changes. In epilepsy, human genetics have revealed mutations in voltage-gated ion channels (channelopathies), synaptic channels (synaptopathies), and metabolic genes in both sporadic[12] and familial[13] disease. Other diseases, such as Alzheimer's Disease (AD) and autism spectrum disorder, also involve changes in neuronal activity. However, it is unclear which of the associated risk genes[14,15] affect neuronal activity, and we lack a systematic and scalable approach to establish the effect of genes on neuronal function.

Classically, interrogation of neuronal activity mechanisms has been accomplished through patch-clamp electrophysiology. This technique is the gold-standard to measure a range of properties, including spontaneous synaptic currents and individual channel kinetics. While powerful, these techniques are limited by the number of neurons that can be interrogated as the researcher must make physical contact with each individual neuron. This requires both a high degree of technical skill and large time investment to evaluate each perturbation.

To measure electrical activity from dozens of neurons in a network simultaneously, researchers have turned to the use of multi-electrode arrays (MEAs) and fluorescent activity probes. MEAs circumvent some of the drawbacks of patch-clamp electrophysiology by measuring local field potentials in a network of neurons but are costly and often sacrifice single-neuron spatial resolution. Alternatively, fluorescence-based indicators of calcium[16] and membrane potential[17,18] also circumvent the throughput constraints of patch-clamp electrophysiology while still providing single-neuron resolution. Furthermore, optogenetics using microbial-opsins provides additional temporal control and the ability to stimulate specific neurons.[19,20] Still, the number of perturbations, genetic or pharmacologic, that can be performed are limited in that each must be done in an arrayed format on high-content imaging plates. Recently, it was shown that calcium oscillations detected using GCaMP6 could be used for multiparametric drug screening in healthy and $SOD1^{A4V}$ motor-neurons differentiated from human iPSCs,[21] however, to our

knowledge, a method capable of comprehensively evaluate genetic modifiers of activity on a genome-wide scale has not been reported.

To enable the scalable characterization of gene function in human cells, we developed CRISPR interference (CRISPRi) and activation (CRISPRa) screening[22] and implemented it in human iPSC-derived cell types relevant for brain function and diseases, including neurons,[23,24] microglia,[25], astrocytes[26], and neuron-glia iAssembloids[27]. These screens allow for unbiased identification of genes and mechanisms underlying cell type specific biological processes. While pooled CRISPR-based screens have been successfully deployed to elucidate neuronal phenotypes such as survival,[23,24,27] transcriptomic states,[23,24] oxidative damage,[24] lysosomal function,[24] and protein aggregation,[28] it has so far not been possible to use pooled CRISPR-based screens to uncover modifiers of neuronal activity. Here, we report a method to uncover modifiers of neuronal excitability in massively parallel screens.

To overcome the challenges in evaluating modifiers of neuronal activity at scale, we developed a pooled screening approach using integration of calcium signal. The fluorescent calcium integrator CaMPARI2 acts as an irreversible record of calcium levels in a neuron by photoconverting while in the presence of high calcium and UV light.[29–32] Based on the ratio of photoconversion in each neuron, the relative level of activity can be discerned by flow cytometry. CaMPARI2 was previously used in a genetic screen to identify modifiers of calcium entry in mouse embryonic fibroblasts[33]. Here, we CaMPARI2 in human iPSC-derived neurons in conjunction with CRISPRi to conduct pooled genetic screens and uncover modifiers of neuronal excitability. We validated hit genes using calcium imaging and patch-clamp methods and generated hypotheses for how these hit genes regulate neuronal excitability.

Results

CaMPARI2 photoconversion provides a ratiometric readout for glutamate-induced activity in human iPSC-derived neurons

To establish a readout of neuronal activity compatible with pooled CRISPR-based screens using fluorescence-activated cell sorting (FACS), we evaluated the utility of the fluorescent calcium integrator CaMPARI2.[32] We introduced a CaMPARI2 transgene into our iPSC line expressing CRISPRi machinery and inducible Ngn2[23] using lentiviral integration followed by clonal selection (Figure 1a). These iPSCs are rapidly differentiated into glutamatergic neurons by doxycycline-induced expression of NGN2, and express dCas9-KRAB for efficient knockdown of genes targeted by a sgRNA.[23]

Synaptic dysfunction is a critical hallmark of many human neurological diseases,[34–38] therefore we focused our efforts on establishing a CaMPARI2-readout for synaptic excitability. To depolarize glutamatergic synapses, we stimulated iPSC-neurons with glutamate after 21 days of differentiation and illuminated with UV light to photoconvert CaMPARI2. We then measured the CaMPARI2 red-to-green fluorescence ratio after glutamate stimulation using both microscopy and flow cytometry (Figure 1b). With

confocal microscopy, we found a robust increase in CaMPARI2 photoconversion in neurons treated with glutamate compared to vehicle control (Figure 1c). Virtually no photoconversion was observed with glutamate treatment in tetrodotoxin (TTX)-treated neurons (Figure 1c). TTX-treated neurons showed similar signal compared to vehicle control suggesting that the baseline synaptic excitability of iPSC-neuron cultures is low.

We tested the dose-response relationship of glutamate and CaMPARI2 photoconversion by flow cytometry (Figure 1d) and found that incubation with 30 μM glutamate for 5 minutes followed by exposure to UV light provided good signal without reaching saturation. This intermediate concentration was chosen to provide dynamic range to enable identification of genetic modifiers that either decrease or increase excitability. Co-incubation of glutamate with APV or NBQX, antagonists for NMDA and AMPA receptors, respectively, demonstrated that the detected calcium release is primarily through AMPA receptors (Figure 1e). Additionally, co-incubation of neurons with glutamate and metabotropic glutamate receptor (mGluR) antagonists modulated neuronal excitability, but full inhibition of signal was achieved only in the presence of APV and NBQX (Extended Data Figure 1b). Treatment with KCl also induced a large CaMPARI2 signal (Extended Data Figure 1c-d), demonstrating that multiple methods of neuronal activation can be interrogated with CaMPARI2. Furthermore, we found that 5 minutes of UV illumination maximized signal (Extended Data Figure 1e). Neuron plating density had a slight effect on the photoconversion outcome at 21 days of differentiation (Extended Data Figure 1f). Five minutes of UV illumination had minimal effects on cell viability during the experimental timeline (Extended Data Figure 1g-h) and treatment with glutamate did not cause acute toxicity (Extended Data Figure 1i).

To better understand how our iNeuron system responds to glutamate, we performed current-clamp recordings while treating with 30 μM glutamate for 5 minutes. We find that iNeurons have a heterogeneous response to glutamate, which we classify into four distinct voltage response profiles (Figure 1f). These include iNeurons that do not fire action potentials when treated with glutamate, including those with small depolarizations (Cell type A; N = 4, 22.2% of total cells), and those with larger depolarizations to membrane potentials above -40 mV (Cell type B; N = 7, 38.9% of total cells). Additionally, we found iNeurons that depolarize and fire action potentials, and upon glutamate wash-out repolarize (Cell type C; N = 2, 11.11% of total cells) or remain depolarized (Cell type D; N = 5, 27.8% of total cells).

Current injection data from these iNeurons before glutamate stimulation show the heterogeneity of intrinsic membrane properties that correlate with the different types of responses to glutamate stimulation (Extended Data Figure 2a-b). Cell types A and B showed a trend towards higher rheobase compared to Cell types C and D (Extended Data Figure 2c, one-way ANOVA, $p = 0.05$). Although Cell types A and B did not generate action potentials with glutamate stimulation, they were capable of firing action potentials with high amplitude current injections. Overall, we found that 30 μM glutamate stimulation for 5 minutes generates diverse responses in iNeurons.

CRISPRi screen for modifiers of neuronal excitability

With this technology in hand, we focused our efforts to study neuronal excitability, which has been implicated in many neurological disorders. Patients with Alzheimer's Disease (AD) have an 8- to 10- fold increase in the risk of seizures,[39,40] with familial early-onset cases having more severe risk,[39] and seizure prevalence has been associated with accelerated cognitive decline.[41] Furthermore, neuronal network dysfunction has been proposed as a critical contributor to AD that occurs decades before clinical symptoms manifest.[42] Epilepsy also shows comorbidity with 5-46% of individuals with autism spectrum disorder (ASD),[38] which is believed to be caused by an imbalance of synaptic excitation and inhibition (E/I balance) or dysfunctional ion channels. Identifying the genetic etiology can help inform precise treatment options for patients;[13,43] however, many of these cases are resistant to current anti-seizure medications and monogenic syndromes are only identified in about 40% of patients with epilepsy.[13] This highlights the need for methods that comprehensively evaluate the functional consequences of genetics on neuronal activity.

To establish CRISPRi screening based on the CaMPARI2 reporter, we generated a custom sgRNA library targeting 1,343 genes selected based on their known or proposed roles in neuronal activity (Supplementary Data Table 1), neurodegeneration, and neurodevelopmental disorders (Supplementary Data Table 2). We designed this library to evaluate our screening paradigm by knocking down known regulators of neuronal excitability and potentially uncover new roles for genes implicated in human diseases. The library targets each gene with 5 independent sgRNAs and contains 250 non-targeting control sgRNAs, resulting in a library of 7,450 different sgRNAs (Supplementary Data Table 3).

We transduced our CaMPARI2-CRISPRi-Ngn2 iPSCs with the lentiviral sgRNA library, selected for transduced iPSCs using puromycin, expanded, and then differentiated into neurons by inducing NGN2 expression with doxycycline (Figure 2a). After 21 days of differentiation, we stimulated neuronal activity with 30 μM glutamate, photoconverted CaMPARI2 with UV light for five minutes using a UV light box, and then dissociated neuronal cultures for FACS. We collected neurons with the highest 35% and lowest 35% CaMPARI2 red/green fluorescence ratio, justified previously by extensive quantitative modeling.[44] We determined the frequency of neurons expressing each sgRNA in the library using next-generation sequencing to determine which sgRNAs cause significant increase or decrease in CaMPARI2 response to glutamate exposure (Figure 2a). We performed this screen in duplicate to identify the most robust hits.

Of the 1,343 genes targeted by our custom sgRNA library, we identified 116 genes for which knockdown decreased synaptic excitability and 37 genes for which knockdown increased synaptic excitability, for a total of 153 hits (Figure 2b, FDR 0.1). We found that

199 the observed hits have Gene Ontology (GO) annotations related to neurotransmitter
200 receptor activity, ion transport, and synaptic transmission (Extended Data Figure 3a).

201 We performed an Over-Representation Analysis (ORA) using WebGestalt[45] to identify
202 enrichment of functional classes of genes among the hits (Figure 2b,c). Of the hits that
203 increased synaptic excitability, GO terms for membrane protein localization, clathrin coat
204 assembly, and negative regulation on ion transmembrane transport were over-
205 represented, potentially highlighting mechanisms related to neuronal homeostasis at the
206 plasma membrane and synaptic vesicle recycling. Additionally, many GO terms related
207 to gene transcription and chromatin regulation (Figure 2c) were over-represented in hits
208 that decrease synaptic excitability, which suggests altered gene expression is important
209 for synaptic function or could be related to delayed neuronal differentiation. The GO term
210 *Cellular Response to Amino Acid Starvation*, an arm of the integrated stress pathway
211 (ISR), was over-represented in hits decreasing synaptic excitability. Previous studies
212 have explored the use of ISRIB, and ISR inhibitor, to restore cognitive deficits in mice.[46]
213 Furthermore, our screen revealed that knockdown of *EIF2AK3, EIF2AK4,* and *ATF4*
214 reduced excitability, in line with previous work showing the role of eIF2a in long-term
215 memory formation.[47,48] These hit genes highlight that neuronal excitability is influenced
216 by diverse molecular pathways and that the CaMPARI2-based screening method is
217 capable of detecting neuronal excitability modifiers that are upstream in these pathways.

218 Many hit genes have been associated with Alzheimer's Disease, epilepsy, and/or
219 autism spectrum disorder (Figure 2d, Extended Data Figure 3b). While our custom library
220 was purposely enriched with these disease-associated genes (Supplementary Data
221 Table 2), this screen suggests a potential, previously unknown role these hit genes play
222 in regulating neuronal excitability.

223 *Validation of screen hits reveals mechanisms of altered excitability including altered*
224 *synaptic function and action potential dynamics*

225 We examined these observed screen phenotypes by flow cytometry using two
226 individual guides targeting *CACNG2* and *KCNT2*, directly comparing the CaMPARI2 ratio
227 after glutamate stimulation of iPSC-neurons receiving the sgRNA versus iPSC-neurons
228 without guide (Figure 3a). This is expressed as a normalized CaMPARI ratio (neuronal
229 excitability), where the mean response of neurons in wells with no sgRNA transduction is
230 equal to one. We evaluated neuronal networks in which 100% of neurons received a
231 sgRNA and networks in which 50% of neurons received a sgRNA which allowed us to
232 evaluate both cell autonomous and cell non-autonomous effects on neuronal excitability.

233 Knockdown of *CACNG2* decreased neuronal excitability in response to glutamate
234 when compared to neurons that were not transduced with the sgRNA (Figure 3a). We
235 tested the effect of this knockdown in neuronal populations where approximately 50% of
236 the neurons expressed an sgRNA and found a robust decrease in excitability in *CACNG2*
237 knockdown neurons compared to intra-well neurons without a sgRNA. In populations
238 where approximately 100% of the neurons had *CACNG2* knockdown, neuronal

239 excitability was dramatically reduced when compared to populations of neurons without
240 sgRNA treatment (Figure 3a). Similarly, with *KCNT2* knockdown we observed increased
241 excitability as observed in the screen (Figure 3a). In populations where all neurons were
242 transduced, there was an overall decrease in excitability, which opposes the screen
243 phenotype and suggests more complicated roles for *KCNT2* via both cell autonomous
244 and network level impacts. Together, these results suggest that the CaMPARI2 screening
245 modality can capture genetic modifiers of activity.

246 Our CaMPARI2-based CRISPRi screening method positively identified modifiers of
247 neuronal excitability, including AMPAR (*CACNG2, GRIA4*) and NMDAR (*GRIN2A*,
248 *GRIN2B*) subunits and ion channels (*KCNT2, CACNA1C, CACNA1D*). To explore
249 neuronal excitability mechanisms that could be detected by the CaMPARI2 screening
250 approach, we evaluated the effects of *CACNG2* and *KCNT2* perturbation using whole-
251 cell electrophysiology. For these experiments, ribonucleoprotein (RNP) mediated
252 CRISPR was used to generate knockouts (KOs) in human iPSC neurons, with NTC
253 guides as negative controls. Recordings of spontaneous excitatory postsynaptic currents
254 (sEPSCs) revealed differences in synaptic activation between *CACNG2* KO neurons and
255 neurons treated with NTCs (Figure 3b, Extended Data Figure 4c,d). A small reduction in
256 the frequency of detected sEPSCs in *CACNG2* KOs was observed compared to NTC
257 (Figure 3c). Furthermore, the half-width and charge transfer of these sEPSCs was
258 significantly attenuated in *CACNG2* KO neurons (Figure 3d-e), reflecting altered receptor
259 kinetics. This decreased synaptic activation observed in the whole cell recordings aligns
260 with previous observations,[49–54] and reflects the reduced excitability observed in the
261 CaMPARI2 screen. These results indicate that the CaMPARI2 screening approach is
262 sensitive to detect known regulators of synaptic excitability with complex
263 electrophysiological phenotypes.

264 We observed no effect on passive membrane properties in *KCNT2* KO neurons
265 (Extended Data Figure 4g-i). However, large current injections caused a drop in action
266 potential firing rate in *KCNT2* KO neurons and premature entry into depolarization block,
267 whereas neurons with a NTC sgRNA do not (Figure 3f-g). These results indicate that in
268 addition to synaptic regulators, the CaMPARI2 screening approach is sensitive to detect
269 regulators of action potential firing such as ion channels.

270 *Modifiers identified in the CaMPARI2 screen are reproducible, specific to neurons, and*
271 *can be stimulus-specific*

272 We generated a focused CRISPRi sgRNA library targeting 395 hit genes
273 (Supplementary Table 4) from our primary screen (based on a relaxed criterion for hit
274 genes, see Methods) for secondary validation screens. We subjected CaMPARI2
275 neurons to either treatment with 30 μM glutamate or 50 mM KCl in two independent
276 screens (Extended Data Figure 3a). We selected 50 mM KCl treatment as it resulted in a
277 CaMPARI2 response with large dynamic range (Extended Data Figure 1c-d). Comparison
278 of gene scores from our primary glutamate-based screen (Figure 2) and our secondary
279 glutamate-based validation screen showed a high degree of correlation (Pearson's R =

280 0.60, Figure 4a), suggesting that the CAMPARI2 screening paradigm produces
281 reproducible results. Many genes had similar effects when knocked down in the
282 secondary glutamate-stimulated screen and the KCl-stimulated screen (Pearson's R =
283 0.33, Figure 4b), suggesting mechanisms that modify neuronal excitability in a general
284 way irrespective of the depolarization method. Still, there were many hits that specifically
285 modified excitability in the secondary glutamate screen, but not in the KCl screen
286 (Extended Data Figure 6f). For instance, *KCNT2* knockdown had no significant phenotype
287 with KCl-mediated depolarization, despite our observation that *KCNT2* KO neurons enter
288 depolarization block prematurely during high levels of current injection (Figure 3f-g).

289 To evaluate if there are modifiers that primarily affect neuronal calcium homeostasis
290 instead of activity, we co-treated CaMPARI2 neurons with 30 μM glutamate and an
291 antagonist cocktail for full GluR blockage (Extended Data Figure 5b). While we found
292 some modifiers that had a statistically significant gene score, comparison of gene scores
293 to the secondary glutamate screen showed no correlation (Pearson's R = -0.004). This
294 would suggest that while some modifiers influence neuronal calcium homeostasis, the
295 underlying signal from this effect is overshadowed by treatment with glutamate and the
296 effects on neuronal excitability.

297 We collected neurons at the start of differentiation (day 0) and after 21 days of
298 differentiation (before stimulation and photoconversion) to identify knockdowns that affect
299 neuronal survival (Extended Data Figure 5c). To assess which hit genes are specific to
300 glutamate-stimulated activity in neurons, we also treated a subset of the sgRNA-
301 transduced undifferentiated iPSCs with glutamate and used the same photoconversion
302 and FACS strategy (Extended Data Figure 5d). In the survival screen, we found 90
303 significant hit genes with a toxic knockdown phenotype in neurons, and 16 protective hits.
304 Comparison to the secondary glutamate screen (Figure 4d) showed little correlation of
305 these effects (Pearson's R = 0.064). Furthermore, we did not identify any significant hits
306 in iPSCs treated with glutamate. Together, these results indicate that the CaMPARI2
307 screen was specific in detecting modifiers of neuronal excitability.

308 While the use of monoculture iPSC-neurons provides a convenient, reductionist
309 system for biological discovery, the physiological immaturity of these neurons make
310 neuronal excitability changes difficult to relate to more advanced systems. It has been
311 established that coculture of iPSC neurons with astrocytes improves the
312 electrophysiological maturation of the neurons. Therefore, we evaluated changes to
313 neuronal excitability in a coculture of the NGN2 neurons with human iPSC-astrocytes
314 (iAstrocytes)[26] by comparing CaMPARI2 signal by flow cytometry and found a slight
315 increase in spontaneous activity signal and higher sensitivity to glutamate (EC_{50} = 12 μM;
316 Extended Data Figure 6a). We also observed a higher spike count in cocultures relative
317 to monocultured iPSC neurons grown on multi-electrode arrays (MEAs) as early as 14
318 days in culture (Extended Data Figure 6b). Furthermore, the synchrony and spike number
319 of these cocultures is disrupted after treatment with tetanus toxin (TeNT; Extended Data
320 Figure 6c-d), suggesting the presence of synaptic transmission.

To assess the ability of the CaMPARI2 system to evaluate modifiers of neuronal excitability in this coculture model, we examined the effect of these modifiers in spontaneously active cultures and when treated with glutamate (Extended Data Figure 5e). There was no correlation of modifiers affecting spontaneous activity in cocultured neurons when compared to the glutamate treated monocultured iPSC-neurons (Figure 4e). However, performing the screen in coculture and using glutamate has a positive correlation (Pearson's R = 0.36) to the screen performed in monocultured neurons (Figure 4f). Knockdown of synaptic genes like *CACNG2* and *GRIA2* decreased excitability in response to glutamate in both monoculture and coculture, while the *KCNT2* KD increased excitability in both. We noticed genes with stronger phenotypes in monoculture than in coculture (i.e. *KCNJ9,* Extended Data Figure 6g) and cases where phenotypes were stronger in coculture (i.e. *GRIN2B*, Extended Data Figure 6g). This may reflect the changes in excitability between culture conditions, however additional mechanistic validation is needed.

Evaluating mechanisms of disease-associated modifiers of excitability

We selected six additional hit genes that have been associated with human neurological disease for additional validation (Figure 5). *NSD1* and *PHF21A*, both of which decreased synaptic excitability in the glutamate screens, are histone modifiers that have been identified as risk genes for ASD. Comparing the CaMPARI2 response in neurons receiving sgRNAs normalized to neurons without a guide, individual knockdown of *NSD1* and *PHF21A* recapitulated the observed phenotype in the screen (Figure 5a). We also validated the screening phenotype for *GRIA2* (Figure 5a), an AMPA receptor subunit that is downregulated after kainate-induced status epilepticus in the hippocampus.[55,56]

We then examined three hits that increased neuronal excitability in the CaMPARI2 CRISPRi screens. *CACNG7* encodes TARP g-7, which is related to stargazing, has been found to be reduced in mouse models of spinocerebellar ataxia type 23 (SCA24).[57] In the screen, *CACNG7* knockdown increased neuronal excitability and we observe a general increase in neuronal excitability in *CACNG7* knockdown neurons in independent experiments (Figure 5b). *PTEN*, classically associated with its role as a tumor suppressor gene[58] and in mitophagy,[59] has been shown to modulate neurite outgrowth and synapse density in *PTEN* KO mice.[60] Furthermore, recent whole-exome sequencing studies have implicated *PTEN* in ASD.[15] In the CaMPARI2 screen, *PTEN* knockdown increased synaptic excitability and *PTEN* knockdown neurons are more excitable when compared to baseline neurons (Figure 5b).

Recently, it has been suggested that *PICALM* may also regulate calcium permeable (CP)-AMPA receptors (AMPARs with homomeric GluA1 subunits) by targeting surface receptors for endocytosis.[61] To test for regulation of CP-AMPARs in human iPSC-neurons, we performed patch clamp recordings in *PICALM* KO and non-targeting control iPSC-neurons. In these experiments we measured AMPA receptor mediated sESPC amplitudes at depolarized and hyperpolarized holding potentials and calculated the

362 rectification index ($sESPC_{AMPAR}$ +40 mV / $sESPC_{AMPAR}$ -70 mV). While a high rectification
363 index indicates few CP-AMPARs, a low rectification index indicates the presence of CP-
364 AMPARs. We found a decrease in the rectification index in *PICALM* KO iPSC-neurons
365 compared to non-targeting control (Figure 5c-e), suggesting that *PICALM KO* increases
366 the level of CP homomeric GluA1 AMPARs at the synapses of human iPSC-derived
367 neurons.

368 *CROP-seq screen connects transcriptional changes to excitability phenotypes*

369 Many of the hits in the glutamate CaMPARI2 screen are known regulators of
370 differentiation, neural development, and have been implicated in neurodevelopmental
371 disorders. To evaluate which of these genes are hits because of changes to neuronal
372 maturation in iPSC-neurons versus bona fide modulator of neuronal excitability, we
373 generated a pooled sgRNA library targeting 45 genes (2 sgRNAs per gene, plus 5 non-
374 targeting controls; SI table 10) that were annotated as being transcriptional regulators,
375 involved in development or differentiation, and were hits in the CaMPARI screen. We
376 introduced the CROP-seq library via lentiviral transduction into iPSCs at a low MOI (0.1)
377 and selected transduced iPSCs with puromycin. These iPSCs were differentiated into
378 neurons, dissociated into a single-cell suspension after 21 days of differentiation and
379 subjected to single-cell RNA sequencing (scRNA-seq). After removing droplets that did
380 not pass quality control cutoffs and only keeping cells with an sgRNA MOI of 1 (Methods),
381 we analyzed 9252 neurons. By combining a transcriptional profile with assignment of a
382 sgRNA for every neuron through sequencing, we could assess the effect of gene
383 knockdowns in a pooled screen.

384 *Marker gene expression and cluster shift analysis does not indicate broad changes in cell*
385 *identity*

386 To examine the effect of knockdown on neuronal identity, we performed Leiden
387 clustering on all 9252 neurons. By uniform manifold approximation and projection (UMAP)
388 for dimensionality reduction, we separated cells into three clusters (Extended Data Figure
389 8a-e) and examined the expression of marker genes (Figure 6a). Doublecortin (*DCX*), a
390 microtubule binding protein associated with the developing cortex, was highly expressed
391 in all neurons. Eomesodermin (*EOMES*), a TBR1 family transcriptional activator critical
392 for progenitor cell proliferation, and DNA topoisomerase II alpha (*TOP2A*), which is a
393 marker for mitotically active cells, showed low expression throughout each cluster. For
394 each neuronal and neural progenitor marker gene, expression was consistent across the
395 defined clusters (Figure 6a), indicating that the clusters do not reflect different stages in
396 neuronal differentiation.

397 Next, we evaluated the effect of each knockdown on the distribution of neurons within
398 the defined clusters relative to the distribution of neurons with non-targeting control
399 sgRNAs. Of the 45 genes examined, only *TRIP12* knockdown showed consistent results
400 across both sgRNAs tested. We observed a significant enrichment of neurons with
401 *TRIP12* knockdown in cluster 2 and a depletion from cluster 0 (Extended Data Figure 8f).

402 We also observed significant cluster enrichment (*RFX3*, *UBR1*) and depletion (*GIGYF2*,
403 *VEZF1*) for individual sgRNAs and large, but statistically insignificant, percent changes in
404 cluster occupancy for additional targets. Together with the consistent marker gene
405 expression across the identified clusters, this suggests that changes in neuronal
406 differentiation trajectory were not the main contributor to the observed changes in
407 neuronal excitability for the hits in the CaMPARI2 screens, but that the hit genes affect
408 neuronal activity through other mechanisms.

409 *Differential Expression Analysis uncovers differences in transcriptional signatures*

410 To determine the transcriptional changes that resulted from each knockdown, we next
411 used the CROP-seq dataset to identify differentially expressed genes (DEGs) by
412 comparing each individual sgRNA knockdown to the group of 5 NTC sgRNAs. 39 sgRNAs
413 had statistically significant knockdown of the intended target gene relative to NTCs
414 (Figure 6b), although almost all sgRNA showed a trend for knockdown of the target gene,
415 suggesting that knockdown was effective for most sgRNA, even if its detection was limited
416 by statistical power. 43 of the 90 sgRNAs had greater than one DEG (Figure 6c). We
417 identified 660 unique DEGs, 196 of which were shared across knockdown of two or more
418 targeted genes.

419 Next, we examined sgRNA groups with on-target knockdown of the target gene
420 (Figure 6b) with at least 10 significantly expressed genes. We performed hierarchical
421 clustering to determine any common DEG signatures across knockdowns and found that
422 pairs of effective sgRNAs targeting the same gene clustered together (Extended Data
423 Figure 8g). However, we did not observe any convergence between DEG signatures of
424 different gene knockdowns, suggesting the knockdowns we selected are acting through
425 different pathways.

426 TRIP12 *knockdown induces transcriptional changes to the synapse*

427 *TRIP12* encodes thyroid hormone receptor interactor 12, an ubiquitin E3 ligase
428 involved multiple ubiquitin-dependent proteolytic pathways[62] and DNA damage repair.[63,64]
429 Mutations in *TRIP12* have been associated with Clark-Baraister syndrome and intellectual
430 disability[64], however it remains unclear which mechanisms lead to the clinical
431 presentation of disease. Given that *TRIP12* knockdown reduced excitability in the
432 CaMPARI2 screen, significantly changed cluster occupancy, and resulted in the most
433 DEGs, we examined the affected pathways caused by *TRIP12* knockdown in our
434 neurons.

435 *TRIP12* knockdown resulted in 213 downregulated and 124 upregulated genes
436 (Figure 6d). We performed gene set enrichment analysis on the upregulated DEGs, which
437 were significantly enriched for GO terms related to ERK1/2 signaling (Figure 6e) and
438 presynaptic changes to synaptic transmission (Figure 6f). Downregulated DEGs showed
439 a significant enrichment for many terms related to synaptic transmission and development
440 (Figure 6e) as well as components of the postsynaptic density (Figure 6f). These changes
441 to the post-synapse, in particular the downregulation of the ionotropic glutamate receptor

442 subunits *GRIA4* and *GRIN2A*, could explain the reduced excitability we observed with
443 *TRIP12* knockdown neurons when treated with glutamate in the CaMPARI2 screen.

444 PTEN *knockdown changes neuronal projection regulation and synaptic vesicle cycling*

445 Finally, we examined *PTEN* knockdown, which increased synaptic excitability in the
446 CaMPARI2 screen and in individual validation experiments (Figure 5b). We found a
447 downregulation of the genes *STMN1*, *STMN2*, and *STMN4* (Figure 6g), which encode
448 stathmins involved in the regulating microtubule polymerization and depolymerization.
449 This could explain previous studies in *PTEN* KO mice, which have enhanced dendritic
450 arborization and additional protrusions compared to control mice.[60] Additionally, gene set
451 enrichment analysis of downregulated genes significantly highlighted Gene Ontology
452 terms related to neuronal projections and microtubule polymerization (Figure 6h). We also
453 performed the same analysis on upregulated genes and found significant enrichment of
454 components of the synaptic vesicle cycle. Specifically, the upregulation of *SNAP25,*
455 *VAMP2, PCLO,* and *SLC17A6* suggests changes in synaptic vesicle trafficking and
456 regulation of SNARE complexes. This could explain both the increased excitability of
457 *PTEN* knockdown neurons in the CaMPARI screen and the increase in frequency of
458 excitatory quanta in *PTEN* KO mice from previous studies.[60]

459

460 **Discussion**

461 Changes in neuronal excitability and synaptic dysfunction appear in many
462 neurodegenerative[34,41,65–67] and neurodevelopmental[35,38,68] disorders. In this work, we
463 developed a screening paradigm using calcium integration as a proxy for neuronal activity
464 to explore how perturbation of genes known to regulate to neuronal activity and/or
465 identified risk genes affect synaptic excitability of iPSC-neurons. We found that we could
466 detect the effect of glutamate receptor subunits, TARPs, and ion channels. These hits
467 were confirmed with patch clamp studies and suggests that mechanisms such as altered
468 depolarization-induced action potential dynamics, altered synaptic receptor kinetics, and
469 changes in AMPA receptor calcium permeability could underlie the observed screen
470 phenotypes. The screens and validation experiment also confirmed that roles in neuronal
471 excitability for disease-linked genes could be detected with this approach.

472 Intriguingly, the CaMPARI2 signal in the primary FACS based screen proved to be a
473 sensitive readout detecting a variety of changes in neuronal properties. This is even more
474 remarkable given the heterogeneous response of individual iPSC-derived neurons to
475 glutamate stimulation (Fig. 1f-h, Extended Data Fig. 2). These findings suggest that
476 CaMPARI2-based CRISPR screens can detect modifiers of neuronal properties that are
477 only present in a subset of the neurons screened, and validates CaMPARI2 as a suitable
478 proxy to capture diverse neuronal phenotypes.

479 The CaMPARI2 screen evaluated the effect of known modifiers of synaptic excitability
480 in iPSC-neurons. Multiple genes belonging to the transmembrane AMPA receptor protein

481 (TARP) family were identified as hits. TARPs are known to influence the density and
482 function of AMPARs.[49,54] The type-I TARP encoded by *CACNG2* has previously been
483 shown to interact with PSD-95 to stabilize AMPARs at the postsynaptic density[51] and to
484 modulate AMPA receptor levels [50,54] and kinetics.[54] Of the six known TARP isoforms,[50]
485 CRISPRi knockdown of *CACNG2* and *CACNG4* reduced synaptic excitability while
486 *CACNG7* knockdown increased synaptic activation in the CaMPARI2 based screen
487 (Figure 2b).

488 Our results indicate that the CaMPARI2 screen is capable of detecting subtle changes
489 to neuronal excitability and can highlight previously under-studied channels for additional
490 characterization. *KCNT2* encodes the sodium-activated potassium channel $K_{Na}1.2$
491 (Slick). Potassium (K^+) channels play a major role in modifying neuronal excitability and
492 regulating synaptic vesicle release,[69] and $K_{Na}1.2$ has been implicated in the adaptation of
493 neuronal firing patterns in auditory neurons.[70] Gain-of-function variants in the $K_{Na}1.1$
494 (Slack) channel encoded by *KCNT1*, a paralogue of *KCNT2*, have been extensively linked
495 to neurodevelopmental disorders (NDD) and epilepsy;[71,72] however, the function of $K_{Na}1.2$
496 is less understood, despite the connection of $K_{Na}1.2$ variants to developmental and
497 epileptic encephalopathy[73] and epilepsy.[74] In our study, knockdown of *KCNT2* increased
498 excitability in iPSC-neurons in the CaMPARI2 screen (Figure 2b) and led to premature
499 depolarization block in current-clamp experiments (Figure 3f-g). This depolarization block
500 may lead to sustained activation of Ca^{2+} channels and lead to an increase in CaMPARI2
501 signal in our screen and flow cytometry experiments with 50% of neurons with *KCNT2*
502 KD. At the same time, in cultures with 100% of neurons with *KCNT2* KO/KD, the reduced
503 numbers of action potentials could lead to reduced network activity which may have a
504 dominant effect in reducing overall excitability that overrides the cell-autonomous
505 increases in calcium influx. This would lead to the decrease in CaMPARI signal we
506 observed by flow cytometry in cultures where 100% of neurons have *KCNT2* KD.
507 However, since we did not investigate the effects on synaptic excitability directly, we
508 cannot rule out potential contributions *KCNT2* may have on synaptic excitability. This
509 could be addressed in the future with additional electrophysiology studies.

510 Evaluating disease risk genes for their role in neuronal activity presents a possible
511 route to developing new therapeutics. *PICALM* encodes the phosphatidylinositol-binding
512 clathrin assembly protein (PICALM), and is originally noted for its involvement in AP2-
513 dependent clathrin-mediated endocytosis.[75,76] GWAS studies have implicated variants at
514 the *PICALM* locus to be associated with late-onset AD,[77,78] which has been verified with
515 additional meta-analysis[79,80] and functionally shown to modify the clearance of tau.[81] We
516 observed an increase in synaptic excitability with *PICALM* knockdown in the CaMPARI2
517 screen with glutamate, and PICALM knockdown increased excitability with the largest
518 effect size of the genes tested in the individual validation experiments (Figure 5b). Other
519 studies have noted late-onset AD risk genes, including *PICALM*, to be involved with
520 synaptic dysfunction[34] and a recent study demonstrated the role of *PICALM* in the
521 regulation of long-term potentiation and memory.[61]

522 To our knowledge, this calcium-integration strategy represents the first pooled
523 modifier screen for neuronal activity. Intriguingly, this strategy uncovered modifiers of
524 numerous aspects of neuronal excitability, including depolarization block, changes to
525 receptor kinetics, and modifications to receptor subunit partitioning at the synapse.
526 Additionally, combining this method with scRNA-seq methods such as CROP-seq
527 identified multiple genes with effects on excitability through changes to transcriptional
528 programs of synaptic genes and neurite growth. Paired together, these complementary
529 methods can identify genetic regulators of neuronal excitability and prioritize them for
530 additional study.

531 While these CRISPRi screens using CaMPARI2 can uncover potentially novel roles
532 for genes in neuronal activity and excitability, we note there are limitations with this
533 method. Primarily, the 405 nm (UV) light needed for CaMPARI2 photoconversion can
534 cause photodamage to cells. We demonstrate that neurons exposed to the five minutes
535 of 405 nm light used in the screen do not undergo massive death or enter apoptosis on
536 the same timescale of the screen, however we acknowledge low cell recovery from FACS,
537 which we attribute to the fragility of these neurons. We were able to overcome this
538 obstacle because of the scalability of our iPSC-neuron system. However, screening the
539 entire protein coding genome will be a major endeavor. To combat this drawback, we plan
540 to incorporate other calcium integration strategies such as scFLARE.[82] This strategy uses
541 488 nm light to initiate activation through a conformational change of the sensor, which is
542 less toxic than UV light. Furthermore, this Ca^{2+} integration strategy can be modified to
543 provide a transcriptional readout,[83] which could be paired with CRISPRi for transcriptional
544 perturbation screens using either the Perturb-seq or CROP-seq method.

545 Another potential drawback of our first application of this approach is the limited
546 functional maturity of iPSC-neurons. We chose to perform these studies after 21 days of
547 differentiation in BrainPhys media, which helps to accelerate maturation of iPSC-derived
548 cultures,[84,85] as this provided a timepoint where the neurons displayed reasonable
549 spontaneous activity while also convenient for screening. Generally, extended maturation
550 times upwards of 9 weeks (>60 days) are needed to develop synaptic maturity in these
551 iPSC-neuron systems[86] and co-culture with astrocytes is needed to enhance the
552 maturation of iPSC-neurons and facilitate increases in activity.[87]

553 In the first application of this CaMPARI2-based pooled screen, we decided focus on
554 synaptic excitability due to prevalence of synaptic defects in many neurological disorders.
555 However, the low correlation between glutamate and KCl screens suggests that this
556 method could be used to detect excitability modifiers through different mechanism. For
557 this reason, it would be informative to perform additional large-scale screens to screen
558 additional mechanisms of neuronal excitability. Furthermore, this screening approach
559 could be adapted to examine neuronal activity in response to other pharmacologic agents
560 like kainic acid to produce seizure-like firing. CaMPARI2 screens could also be used to
561 evaluate electrophysiological maturation of iPSC-neurons longitudinally or to probe
562 mechanisms of plasticity. Optogenetic tools that are spectrally compatible with

563 CaMPARI2 could be used in this paradigm to examine how particular genes affect specific
564 firing patterns of neurons.

565 We believe that our CaMPARI2-based CRISPRi screening platform will help to
566 uncover the functional roles of risk genes for many different neurological disorders of both
567 the central and peripheral nervous systems. The development of new differentiation
568 protocols and increased availability of iPSC models provides an opportunity to extend this
569 paradigm to other specialized types of neurons, such as motor neurons and inhibitory
570 neurons, and to patient-derived iPSC-neurons with disease-linked mutations. Beyond
571 astrocytes, other cell types could also be incorporated into 2D or 3D culture systems,
572 such as iAssembloids.[27] Understanding the genetic determinants of neuronal activity in
573 different contexts will lead to an understanding of disease mechanisms related to aberrant
574 neuronal activity potential and the development of new therapeutics.

575

576 **Methods**

577 **Human iPSC Culture**

578 hiPSCs were cultured in StemFlex medium (Thermo Fisher Scientific, A3349401) in
579 plates or dishes coated with Growth Factor Reduced, Phenol Red-Free, LDEV-Free
580 Matrigel Basement Membrane Matrix (Corning, 356231) diluted 1:100 in Knockout DMEM
581 (Thermo Fisher Scientific, 10829–018). StemFlex medium was replaced daily. Upon 70-
582 80% confluence, hiPSCs were dissociated to single-cell suspensions with StemPro
583 Accutase Cell Dissociation Reagent (Thermo Fisher Scientific, A1110501). hiPSCs were
584 washed with Dulbecco's Phosphate Buffered Saline without $CaCl_2$ and $MgCl_2$ (Sigma,
585 D8537-24X500ML), incubated with Accutase for 3-7 minutes at 37°C until cell could be
586 dislodged with gentle trituration. The cell suspension was diluted 5x with DPBS,
587 transferred to tubes, and centrifuged at 200xg for 5 minutes. hiPSCs were resuspended
588 in StemFlex Medium supplemented with 10 nM Y-27632 dihydrochloride ROCK inhibitor
589 (Tocris Bioscience, 1254), counted, and plated onto Matrigel-coated plates or dishes.
590 hiPSCs were maintained in Y-27632 until colonies reached the appropriate size (more
591 than 15 cells/colony). Studies with human iPSCs at UCSF were approved by the Human
592 Gamete, Embryo, and Stem Cell Research (GESCR) Committee. Informed consent was
593 obtained from the human subjects when the hiPSC lines were originally derived.

594

595 **Generation of CaMPARI2 hiPSC line**

596 To generate CaMPARI2 iNeurons, the CaMPARI2 gene (1446 bp) was subcloned from
597 pAAV_hsyn_NES-his-CaMPARI2-WPRE-SV40 (Addgene 101060, gift from Eric
598 Schrieter)[32] into a lentiviral plasmid (pRT050) under a CAG promoter and an upstream
599 UCOE element via Gibson Assembly to yield pRT074. iPSCs expressing CRISPRi
600 machinery and inducible NGN2[23] were transduced with lentivirus delivering pRT074

601 (described in more detail below). Clonal lines were isolated by colony picking,
602 differentiated to neurons, and evaluated for homogeneity of CaMPARI2 expression and
603 dynamic range of photoconversion. A clonal line satisfying the above criteria was selected
604 for CaMPARI2 photoconversion experiments and screening.

605

606 **Lentiviral transduction of iPSCs**

607 *CaMPARI2 (pRT074)*

608 pRT074 was lentivirally packaged in HEK 293T cells (ATCC Cat. No. CRL-3216) DMEM
609 complete medium: DMEM (Gibco, 11965-092) supplemented with 10% FBS (VWR,
610 89510, lot: 184B19), 1% penicillin-streptomycin (Gibco, 15140122), and 1% GlutaMAX
611 (Gibco, 35050061) as described previously,[23] using TransIT Lenti Transfection Reagent
612 (Mirus Bio; Cat. No. MIR 6600) according to manufacturer's protocol.

613

614 *sgRNA constructs*

615 Individual or pooled sgRNAs were lentivirally packaged in HEK 293T cells (ATCC, CRL-
616 3216) in DMEM complete medium as described previously[23] with the following
617 modifications: a 3:1 ratio of 1 µg/µl polyethenylamine (PEI) (Linear, MW 25,000,
618 Polysciences, 23966) to transfer DNA was used in place of TransIT Lenti Transfection
619 Reagent. Cells were selected with 0.8 µg/mL puromycin (Gibco; Cat. No. A11138-03) for
620 2 days until the fraction of infected cells was > 0.95, as determined by flow cytometry of
621 sgRNA-BFP fluorescence. Additional rounds of puromycin selection were used as
622 necessary until the fraction of infected cells was above 0.95, after which cells were
623 cultured for a single passage in the absence of puromycin to allow them to recover.
624 sgRNA protospacer sequences are provided in Supplementary Table 7.

625

626 **iNeuron differentiation and culture**

627 *For screening, flow cytometry, and imaging*

628 hiPSCs were differentiated into iNeurons according to Tian et al.[23] At day 0 of
629 differentiation, iNeurons were plated onto poly-D-lysine-coated plates (Corning 6W
630 356413, 12W 356470, 24W 354414, 96W 354640, 15cm 354550) in BrainPhys neuronal
631 media (composed according to Bardy et al. 2015)[84] and 2 µg/ml doxycycline (Takara
632 631311). Three days after plating and, later, twice weekly, half of the culture media was
633 removed and replenished with freshly supplemented BrainPhys without doxycycline.
634 iNeurons were cultured for 21 days for all activity experiments.

635

636 *For electrophysiology with wild-type NGN2 iNeurons or RNP-CRISPR mediated*
637 *knockouts (KO)*

638 Human iPSCs from iP11N background (ALSTEM) with inducible expression of Ngn2 by
639 doxycycline (Dox) were differentiated into neurons using combined Ngn2 programming
640 and dual SMAD patterning according to optimized from a previously published
641 protocol.[88,89] The iPSCs were cultured in mTeSR plus media for maintenance and in
642 initiation media (F12/DMEM media, N2, B27 without VA, glutamax, NEAA) for
643 differentiation. On day 7 of differentiation, Ngn2 iNeurons were further cultured in neuron
644 maturation medium (iCell Neural Base medium 1 CDI M1010, iCell Neural Supplement B
645 CDI M1029, iCell Nervous system Supplement CDI M1031) for more than 14 days before
646 electrophysiology measurements were made.

647 **iAstrocyte differentiation and culture**

648 Neural progenitor cells (NPCs) were first differentiated as previously described,[26] then
649 iAstrocyte differentiation was initiated by seeding NPCs into ScienCell Astrocyte Media
650 (ScienCell Research Laboratories, 1801) + 2 µg mL^{-1} doxycyline.[26] Media was changed
651 every other day, with doxycycline maintained at 2 µg mL^{-1} throughout the differentiation
652 process. At day 15, iAstrocytes were cryopreserved in ScienCell Astrocyte Media + 10%
653 DMSO.

654 **Coculture of iNeurons and iAstrocytes**

655 At day 0 of the iNeurons differentiation, day 15 iAstrocytes were thawed and resuspended
656 in ScienCell Astrocyte media. iNeurons were dissociated and resuspended in BrainPhys
657 neuronal media (see above). At a final seeding density of 2:1 iNeurons:iAstrocytes (468k
658 iNeurons + 234k iAstrocyte per cm^2), these cells were mixed in a 1:1 ratio of BrainPhys
659 neuronal media: ScienCell Astrocyte media + 2 µg mL^{-1} doxycycline and seeded onto
660 PDL + laminin coated dishes. After 3 days, a full media change into BrainPhys neuronal
661 media was performed, followed by a half change with BrainPhys neuronal media every
662 other day until the experimental timepoint.

663 For flow cytometry and FACS, these cultures were dissociated with the same method as
664 monocultured neurons (see above), and neurons were gated using the CaMPARI green
665 fluorescence.

666 **RNP-CRISPR knockouts**

667 On day 7 of differentiation, cells were lifted by Accutase (Stemcell technology) and
668 resuspended in P3 buffer (Lonza). RNP were prepared by mixing Cas9 (Alt-R™ S.p. Cas9
669 Nuclease V3, IDT) and gRNA for *KCNT2*, *CACNG2*, *PICALM* (Synthego KO kit) and non-
670 targeting control (NTC) sequences (Genentech) separately. KO kits were used as a pool
671 of three sgRNAs/gene (protospacer sequences are provided in Supplementary Table 6).
672 These were then incubated at room temperature for 20 min. iNeurons in P3 buffer were
673 then mixed with Cas9 RNP and nucleofected using pulse program CV-110 in the 4D-
674 Nucleofector (Lonza). After nucleofection, iNeurons were plated at 1M in poly-D-lysine
675 (A38904-01, Gibco) and iMatrix (T304, TaKaRa) coated µ-dishes (Cat. No. 80136, ibidi)
676 for electrophysiology and further cultured in neuron maturation medium (iCell Neural Base

677 medium 1 CDI M1010, iCell Neural Supplement B CDI M1029, iCell Nervous system
678 Supplement CDI M1031) for more than 14 days before electrophysiology measurements
679 were made.

680

681 **iNeuron dissociation protocol for flow cytometry**

682 Dissociation solution was made from resuspending papain (Worthington; Code: PAP2;
683 Cat. No.LK003178) in 1X Hank's Balanced Salt Solution (Corning; Cat. No. 21-022-CV)
684 to 20 U/mL. 5 mM $MgCl_2$ and 10 U/mL DNaseI (Worthington; Code: DPRF; Cat. No.
685 LS006333) were then added to the solution. Dissociating solution was added to 96-well,
686 24-well, 12-well, 6-well plates and 15 cm dishes at volumes of 20 µL, 100 µL, 250 µL, 500
687 µL, and 5 mL, respectively. iNeurons were treated with dissociation solution for 12
688 minutes at 37ºC and resuspended in 1X Hank's Balanced Salt Solution (HBSS, Gibco)
689 before analysis.

690

691 **CaMPARI2 photoconversion**

692 CaMPARI2 iNeurons plated on poly-D-lysine coated cell culture plates were illuminated
693 with 405 nm light (LED output 39 W) in a temperature-controlled box with rotating
694 turntable (FormLabs FH-CU-01). After 5 minutes of illumination at 37ºC, iNeurons were
695 dissociated (see above) or imaged.

696 For imaging CaMPARI2 photoconversion, CaMPARI2 iNeurons were plated onto 96-well
697 poly-D-lysine coated plates (Corning 354640) at 25,000 cells/well (78,000 cells/cm^2) in
698 BrainPhys neuronal media. On day 21, iNeurons were treated with 30 µM glutamate, 1.5
699 mM tetrodotoxin, or 0.1% DMSO (Vehicle) for 5 minutes at 37 ºC. After photoconversion
700 (see above), iNeurons were imaged on an ImageXpress Micro Confocal High-Content
701 Imaging System (Molecular Devices) using an Apo LWD 20X/0.95NA water immersion
702 objective. Laser settings: Hoechst 33342 - EX 405/20 nm, EM 452/45 nm with FF409-
703 Di03 dichroic; CaMPARI2-green - EX 467/21 nm; EM 520/40 nm with ZT
704 405/470/555/640/730 dichroic; CaMPARI2-red – EX 555 nm, EM 598/40 nm with ZT
705 405/470/555/640/730 dichroic.

706

707 **CaMPARI2 photoconversion experiments for flow cytometry**

708 CaMPARI2 iNeurons were plated onto 96-well poly-D-lysine coated plates (Corning
709 354640) at 25,000 cells/well (78,000 cells/cm^2) in BrainPhys neuronal media. On day 21,
710 iNeurons were treated with 30 µM glutamate, 1.5 mM tetrodotoxin, or 0.1% DMSO for 5
711 minutes at 37 ºC. iNeurons were then photoconverted with UV light and dissociated as
712 described above before analyzing them by flow cytometry using a BD LSRFortessa X14
713 (BD Biosciences) using BD FACSDiva (v.8.0.1.1) software. Flow cytometry data was
714 analyzed using FlowJo analysis software (v10.10.0; BD Life Sciences; Ashland, OR,

715 USA), R/G ratio was calculated for each event captured as the ratio of FITC and mCherry.
716 Mean R/G was calculated for subsequent analyses of CaMPARI2 photoconversion.

717

718 **Toxicity assays**

719 CaMPARI2 cells at Day 0 of differentiation were plated in triplicate at 80,000 cells per well
720 onto 24-well (42k cells/cm^2) poly-D-lysine-coated cellware (Corning 354414) in 400 µl/well
721 of supplemented BrainPhys media. After 21 days of differentiation, CaMPARI iNeurons
722 were UV illuminated for 0, 1, 5, 15, and 60 minutes. Viability was analyzed immediately
723 after and 24 hours after UV exposure. CaMPARI2 iNeurons were dissociated as above,
724 pelleted at 300xg for 5 minutes, and resuspended in 20 µl 1X HBSS, combined with 20
725 µL 0.4% Trypan Blue (Invitrogen T10282), and counted on a Countess II automated cell
726 counter (Invitrogen AMQAX1000) to quantify viable cells.

727 CaMPARI2 iNeurons were plated onto 96-well poly-D-lysine coated plates (Corning
728 354640) at 25,000 cells/well (78,000 cells/cm^2) in BrainPhys neuronal media. On day 21,
729 these were illuminated with UV for 0, 1, 5, 15, or 30 minutes. To perform viability staining
730 with TO-PRO-3 (ThermoFisher T3605), CaMPARI2 iNeurons were washed 3x with
731 DPBS, stained with TO-PRO-3 diluted 1:1000 in DPBS and 1 µM Hoechst 33342 (Thermo
732 Fisher 62249) nuclear counterstain for 30 minutes at room temperature. After staining,
733 cells were washed 3x with DPBS and imaged on an ImageXpress Micro Confocal High-
734 Content Imaging System (Molecular Devices) using an Apo LWD 20X/0.95NA water
735 immersion objective. Laser settings: TO-PRO-3; EX 638/17 nm, EM 624/40 nm with ZT
736 405/470/555/640/730 dichroic; Hoechst 33342; EX 405/20 nm, EM 452/45 nm with
737 FF409-Di03 dichroic. Images were analyzed and cells were segmented using CellProfiler
738 (v 4.2.4) analysis software. TO-PRO-3 staining intensity per object was measured and
739 difference in signal between TO-PRO-3 stained versus unstained cells provided basis for
740 live/dead cell filtering. After filtering live and dead cells, the proportion of live cells was
741 used for viability analysis.

742

743 **Glutamate titration**

744 After 21 days of differentiation, CaMPARI2 iNeurons were treated with increasing
745 concentrations of glutamate (0-500 µM) for 5 minutes. This was followed by CaMPARI
746 photoconversion and dissociation (protocols as described above). The mean R/G ratio
747 for each concentration, with 6 independent culture wells per measurement, was used to
748 calculate a polynomial fit using Prism (v10.1.1). 30 µM was chosen for subsequent
749 experiments and screens due to the potential dynamic range available to detect increases
750 in activity (increase CaMPARI2 response) while still allowing for some dynamic range to
751 sense decreases in activity (lower CaMPARI2 response).

752

753 **CRISPR screens**

754 *Generation of sgRNA library*

755 A custom CRISPRi library targeting genes associated neurological disease and activity
756 (Neuron Activity library) was synthesized as follows: The disease-associated gene list
757 were generated using DisGeNET[90] online database, using the neurodegenerative,
758 neurodevelopment, and neuropsychiatric diseases highlighted in Figure 2c as search
759 terms. This was supplemented using genes chosen by searching terms 'synapse',
760 'neurotransmitter', 'calcium', 'membrane potential', 'neuron activity', and 'neuron
761 membrane' in GO, KEGG, Reactome and Wikipathways. This gene list was filtered for
762 gene expressed in NGN2-iNeurons based of RNA sequencing data,[23] resulting in a final
763 number of 1343 genes targeted in the library. The top 5 predicted sgRNAs[91]
764 oligonucleotide sequences per gene plus 250 non-targeting control (NTC) sequences (for
765 7450 total library elements) were synthesized by Agilent Technologies
766 (RRID:SCR_013575; Santa Clara, CA) on a 7.5K oligo array and cloned into the pLG15
767 sgRNA expression vector. Library complexity and the presence of each oligo was
768 confirmed with Illumina next-generation sequencing.

769 *Primary FACS based screen*

770 The Neuron Activity library was packaged into lentivirus as previously described for the
771 CRISPRi genome-wide sublibraries.[23] CRISPRi-NGN2-CaMPARI2 iPSCs were infected
772 by the sgRNA library at MOIs between 0.3-0.5 (as measured by the BFP fluorescence in
773 the sgRNA lentiviral vector) with >1000X coverage per library element. On the next
774 passage, iPSCs expressing the sgRNA vector were selected using puromycin (see
775 above) as they were expanded for screening, limiting the total number of passages from
776 lentiviral transduction to three to limit dropout of sgRNAs at the iPSC stage. The sgRNA
777 library has a puromycin resistance gene driven from the strong EF1alpha promoter and
778 confers resistance to high levels of puromycin compared to the low levels of expression
779 of this gene from the NGN2 cassette that transcribed as part of the endogenous AAVS1
780 locus. This enables us to re-use puromycin resistance for selection of iPSCs transduced
781 with the sgRNA construct. iPSCs were scaled to a cell count corresponding to >$10e^4$ x
782 coverage per library element for each FACS sorted population, and differentiated into
783 neurons as described above. On day 0 of the differentiation, iNeurons were plated onto
784 15 cm poly-D-lysine-coated plates (Corning 354550) at a density of 138k/cm^2. iNeurons
785 were maintained as described above until FACS sorting.

786 On day 21, iNeurons were treated with 30 μM glutamate for 5 minutes before
787 photoconversion (described above). These were then dissociated with the above
788 dissociation protocol, with the following modifications: incubation time in dissociation
789 solution was increased to 20 minutes, papain was resuspended in 1:1 HBSS and
790 Accutase, and dissociated neurons were resuspended in FACS wash buffer: 20 mL HBSS
791 supplemented with 5 mM $MgCl_2$, 10 nM Y-27632, and 10 U/mL DNaseI. Resuspended
792 iNeurons were maintained as a sheet, transferred to a 50 mL tube, vigorously triturated,

then pelleted at 300xg for 10 minutes. After the supernatant was discarded, the pellet was resuspended in 1-2 mL of FACS wash buffer, using trituration to make a single-cell suspension. Resuspended iNeurons were sorted into high and low R/G ratio populations corresponding to the top 35% and bottom 35% of the R/G signal distribution (see gating strategy, Supplementary Information), followed by sample preparation for next-generation sequencing. This screen was conducted in duplicate.

Pooled secondary screens

The focused secondary screening library contained 1211 sgRNAs targeting 411 genes (3-5 sgRNAs per gene) that were hits in either of the replicate primary screens and 250 NTC sgRNAs (1622 total sgRNAs). sgRNAs were selected based on their phenotype in the primary screens. A pool of sgRNA-containing oligonucleotides were synthesized by Twist Biosciences (South San Francisco, CA, USA) and cloned into an optimized sgRNA lentivirus vector (pMK1334) as previously described.[24] CRISPRi-NGN2-CaMPARI2 iPSCs were transduced with lentivirus containing the secondary screening library, selected, and expanded as described for the primary screen above. A fraction of day 0 iNeurons were harvested and subjected to sample preparation for next-generation sequencing.

On day 21, iNeurons were treated with either 50 mM KCl or 30 μM glutamate, undergoing the same screening protocol as above.

Separately, CRISPRi-NGN2-CaMPARI2 iPSCs transduced with lentivirus were treated with 30 μM glutamate to match the same photoconversion conditions as day 21 iNeurons. These were then dissociated with Accutase (see Human iPSC Culture subsection) and sorted into high and low R/G ratio populations corresponding to the top 35% and bottom 35% of the R/G signal distribution, followed by sample preparation for next-generation sequencing.

Screen sample preparation

For each screen sample, genomic DNA was isolated using a Macherey-Nagel Nucleospin Blood kit (Macherey-Nagel; Cat. No. 740951.50) or Macherey-Nagel Nucleospin Blood L kit (Macherey-Nagel; Cat. No. 740954.20), depending on the number of cells recovered from FACS. sgRNA-encoding regions were amplified and sequenced on an Illumina HiSeq- 4000 as previously described.[23]

Validation of CRISPR screen hits

CaMPARI2 iNeurons expressing sgRNAs targeting hit genes were plated onto 96-well poly-D-lysine coated plates (Corning 354640) at 12,500 cells/well in BrainPhys neuronal media. The assay was internally controlled by plating an equal mixture of CaMPARI2 iNeurons expressing no sgRNA and knockdown iNeurons, to a final density of 25,000 cells/well (78,000 cells/cm^2).

831

832 **qPCR**

833 To quantify knockdown in CaMPARI2 cells, lysed cell pellets from human iPSCs or
834 iNeurons were thawed on ice, and total RNA was extracted using Quick-RNA Miniprep
835 Kit (Zymo; Cat. No. R1054). Complementary DNA was synthesized with the SensiFAST
836 cDNA Synthesis Kit (Bioline; Cat. No. 65054). Samples were prepared for qPCR in
837 technical triplicates in 10-µl reaction volumes using SensiFAST SYBR Lo-ROX 2X Master
838 Mix (Bioline; Cat. No. BIO-94005), custom qPCR primers from Integrated DNA
839 Technologies used at a final concentration of 0.2 µM and cDNA diluted at 1:3. qPCR was
840 performed on an Applied Biosystems QuantStudio 6 Pro Real-Time PCR System using
841 QuantStudio Real Time PCR software (v.1.3) with the following Fast 2-Step protocol: (1)
842 95 °C for 20 s; (2) 95 °C for 5 s (denaturation); (3) 60 °C for 20 s (annealing/extension);
843 (4) repeat steps 2 and 3 for a total of 40 cycles; (5) 95 °C for 1 s; (6) ramp 1.92 °C s^{-1} from
844 60 °C to 95 °C to establish melting curve. Expression fold changes were calculated using
845 the ΔΔCt method, and normalized to housekeeping gene *GAPDH*. Primer sequences are
846 provided in Supplementary Table 5.

847

848 **Electrophysiology**

849 Patch clamp electrophysiology measurements were made using a Multiclamp 700B
850 amplifier, with pClamp10 acquisition software (Molecular Devices). Recordings were
851 filtered at 2 kHz for voltage clamp or at 10 kHz for current clamp. Digitization was
852 performed at a frequency of 10 kHz, with a Digidata 1440 analog-to-digital converter
853 (Molecular Devices). For current clamp recordings the intracellular solution was
854 composed of (in mM): 130 K-gluconate, 5 NaCl, 10 HEPES, 0.2 EGTA, 2 $MgCl_2$, 4 Na-
855 ATP, 0.5 Mg-GTP, with a pH of 7.3. For voltage clamp recordings, the intracellular solution
856 was composed of (in mM): 130 $CsMeSO_3$, 4 NaCl, 10 HEPES, 0.2 EGTA, 5 QX-314 Br,
857 4 Na-ATP, 0.5 Mg-GTP, with a pH of 7.3.

858

859 The recording chamber was continuously infused with oxygenated ACSF, which
860 contained (in mM): 127 NaCl, 2.5 KCl, 1.25 $NaHPO_4$, 25 Na_2CO_3, 25 glucose, 2.5 CaCl2,
861 1.3 MgCl2. Recording electrodes had an open-tip resistance between 4-8 MW. These
862 recordings were performed 2-3 weeks after iNeurons culture media were switched to
863 maturation medium or after the RNP-CRISPR knockout procedure. Data for each gene
864 was collated from two batches of iNeuron cultures.

865 For examining effects of glutamate stimulation on iNeurons using electrophysiology, the
866 current-spike output relationship was measured first as follows: Cells were current-
867 clamped at -70 mV. A sequence of 20 x 1 second long current steps were injected, starting
868 from -20 pA and increased by 10 pA for each step. Then, cells were recorded at their
869 resting membrane potential and 30 µM glutamate in ACSF was washing in for 5 mins with
870 flow speed adjusted to ~2.5 ml/min to have recording chamber solution (~4 ml)
871 exchanged < 2 mins. Finally, cells were then subjected to perfused current-spike output

relationship measurement again after perfusing aCSF for > 8 mins to monitor washout of glutamate.

Specific electrophysiology protocols for individual validation of hit genes:

For the *KCNT2* knockout and NTC iNeurons, the current-spike output relationship was measured as follows: Cells were current-clamped at -70 mV. A sequence of 20 x 1 second long current steps were injected, starting from -20 pA and increased by 10 pA for each step.

For *CACNG2* knockout and NTC iNeurons, spontaneous excitatory postsynaptic currents (sEPSC) were recorded for 1 minute while the cells were voltage clamped at -70 mV. In cases where no events were observed during the initial minute, an additional minute of recording was performed. To enhance the detection of synaptic events, the synaptic vesicle release probability was increased in these experiments by elevating KCl to 5 mM and CaCl2 to 4 mM with zero MgCl2 in ACSF.

For *PICALM* knockout and NTC iNeurons, cells were voltage clamped at -70 mV and +40 mV for one minute to measure sEPSCs. If no events were observed within the initial minute, the recordings were performed for an additional minute. AMPA receptor-mediated sEPSCs were isolated by adding either 50 µM D-AP5 or 100 µM DL-AP5 (Cat. No. 0106Tocris) to the recording solution. Addition of 100 µM cyclothiazide (Cat. No.0713, Tocris or Cat. No. ALX-550-338-M050 Enzo) was used to reduce AMPA receptor desensitization and facilitate the detection of synaptic events. 100 µM spermine (Cat. No. S3256 Sigma-Aldrich) was included in the intracellular solution to block calcium-permeable AMPA receptors at +40 mV, aiding in the quantification of the rectification index (mean sEPSC current amplitude at +40 mV / mean sEPSC current amplitude at -70 mV).

All recordings were analyzed using either Easy Electrophysiology software (v2.6 or v2.7, Cambridge, UK) or Clampfit (v10.7, Molecular Devices; San Jose, CA, USA). The minimum current step that initiated action potential firing was defined as the rheobase. The maximum firing rate was calculated at the current step that initiated the highest number of action potentials, with no failure being observed. The action potential half-width was computed from the first action potential at the rheobase. Recordings were included for analysis if a minimum of 5 sEPSC events were detected during the recording time frame (0.08Hz). Charge transfer for each recording was computed as the frequency * 60 seconds * the charge transfer for the average sEPSCs. Statistical analyses were performed using GraphPad Prism (v10.1.1; GraphPad Software; Boston, MA, USA) including the Mann-Whitney test or an ANOVA, followed by the Kruskal-Wallis test for multiple comparisons.

CROP-seq

CROP-seq sgRNA library construction

We selected genes that were hits in the CaMPARI2 screen that are known regulators of transcription and chromatin, plus control hit genes (e.g. *KCNT2*, *CACNG2*) for a total of 45 target genes. The top two performing sgRNAs from the CaMPARI2 screens were selected for each target. Five non-targeting control sgRNAs were added, resulting in a 95 sgRNA library (SI table 10).

Top and bottom oligo sequences for each sgRNA were ordered in an array from IDT, annealed in a 96 well plate, and then pooled. A 1:20 dilution of this pool was cloned into the CROP-seq vector pMK1334 via BstXI and BlpI restriction sites. To test ligation efficiency, a test transformation was performed in DH5alpha cells. This was followed by a large-scale transformation in Stellar Competent cells for final library amplification and purification. Before transducing cells, we measured the proportion of each sgRNA in the library through sgRNA enrichment PCR and next-generation sequencing to check sgRNA representation in the library and confirm a normal distribution.

Cell preparation

We produced a pool of lentiviruses containing the CROP-seq sgRNA library and transduced iPSCs at a low MOI (10% transduction efficiency) to minimize multiple infections in which a cell receives more than one sgRNA. Then, iPSCs were selected with puromycin (see above), differentiated into neurons, and grown to the same day 21 timepoint used for CaMPARI2 screen. These cells were dissociated in the same manner using papain, then pelleted at 300 xg for 5 minutes. These were resuspended and washed in dPBS. The centrifugation and wash steps were repeated for a total of 4 washes to completely remove papain, DNase, and cell debris. The resuspension was counted and diluted to target 20k cells for a single 10X Chromium GEM-X 3’ chip. Cells were prepared according to 10x Genomics general sample preparation protocol.

Single cell RNA-seq library preparation

20k cells were loaded into a single well of a 10X Chromium GEM-X 3’ chip for GEM preparation. Single cell library preparation was conducted according to the protocol provided for Chromium GEM-X Single Cell 3’ Reagent Kit v4 (10x Genomics, Cat#PN-1000686, User Guide CG000731 Rev A). Concentrations of libraries were measured using Agilent TapeStation D5000 reagents (Agilent Technologies, Cat#5067-5588) on an Agilent 4200 TapeStation system.

sgRNA enrichment

Briefly, three semi-nested PCR reactions were performed followed by 1x SPRIselect beads (Fisher Scientific, Cat#NC0406407) cleanup after each PCR reaction. In PCR1, 15ng full-length cDNA from single cell RNA-seq library prep per sample was used as a template. In PCR2, 10ng post-cleanup PCR1 product was used as a template. In PCR3, 10ng post-cleanup PCR2 product was used as a template to add sample indices. ll PCR reactions were conducted using KAPA Hotstart HiFi ReadMix (VWR, Cat#103568-584) with annealing temperature at 62°C (15 sec) and extension at 72°C (15 sec) for 18 cycles

958 (PCR1) or 15 cycles (PCR2 and PCR3). Concentrations of post-PCR3 products were
959 measured using Qubit dsDNA HS assay kit (Thermo Scientific, Cat#Q32854).
960

Reaction	Primer 1 name	Primer 1 sequence	Primer 2 name	Primer 2 sequence
PCR 1	oRT316_enrichment_pcr_1_r1	CTACACGACGCTCTTCCGATCT	oRT318_enrichment_pcr_1_f	TCGCACGGACTTGTGGGAGAAG
PCR 2	oRT319_enrichment_pcr_2_r	AATGATACGGCGACCACCGAGATCTACACTCTTTCCCTACACGACGCTC	oRT320_enrichment_pcr_2_f	GTGACTGGAGTTCAGACGTGTGCTCTTCCGATCTAGTATCCCTTGGAGAACCACCTTG
PCR 3	oRT319_enrichment_pcr_2_r	AATGATACGGCGACCACCGAGATCTACACTCTTTCCCTACACGACGCTC	oRT321_enrichment_pcr_3_f_index1_E3	CAAGCAGAAGACGGCATACGAGATCAATACCTGTGACTGGAGTTCAG

961
962 *Sequencing*

963 Samples of single cell RNA-seq libraries and enriched sgRNAs were pooled together at
964 5nM for sequencing on one lane of a 10B flow cell of an Illumina NovaSeqX following the
965 recommendations from 10X Genomics. Approximately 1 billion and 400 million reads
966 were generated for the gene expression and sgRNA enrichment libraries, respectively.

967 **Data Analysis**

968 **CRISPR screen analysis**

969 Primary screens were analyzed using sgcount and crispr_screen, two publicly available
970 Rust packages based on MAGeCK[92] and our previously published MAGeCK-iNC
971 bioinformatics pipeline.[23] The packages sgcount and crispr_screen are available on the
972 Kampmann Lab website (https://kampmannlab.ucsf.edu/sgcount,
973 https://kampmannlab.ucsf.edu/crisprscreen) and on Github
974 (https://github.com/noamteyssier/sgcount,
975 https://github.com/noamteyssier/crispr_screen).

976 Briefly, raw sequencing reads from next-generation sequencing are analyzed for the
977 variable region (sgRNA protospacer sequence). Sequences in each sample are cropped
978 to remove adapter regions and non-variable sequences to leave protospacer sequences
979 remaining. These are then mapped to a sgRNA reference library to generate a count
980 matrix for each screen sample. The quality of each screen was assessed by plotting the
981 $\log_{10}$(counts) per sgRNA on a rank order plot using ggplot2.

982 Log_2 fold change and significance P values were calculated for target genes over
983 'negative-control-quasi-genes', as well as an FDR given the 'negative-control-quasi-
984 genes' that were generated by random sampling with replacement of five NTC sgRNAs
985 from all NTC sgRNAs (iNC method). A 'Gene Score' was defined as the product of log_2
986 fold change and −log10(P value). Hit genes were determined based on the p value cut-
987 off corresponding to an empirical false discovery rate of 10%. Volcano plots of log_2 fold
988 change vs $-log_{10}$(p value) and scatter plots of Gene Scores were generated using ggplot2.

989 **Over-representation analysis with WebGestalt**

990 Hit genes from the primary screen were separated into hits decreasing and increasing
991 activity. These lists were input into WebGestaltR[45] (version 0.4.6) and enriched with the
992 ORA method. The screening library was used as the reference gene list. Significant terms
993 were thresholded at a FDR of 0.1, using Benjamini Hochberg.

994 **Image analysis with CellProfiler**

995 Pipelines and example images are compiled in supplementary material, and all analyzes
996 were performed using CellProfiler v.4.1.3. Cell toxicity by TO-PRO-3 co-localization:
997 Nuclei were segmented as primary objects from Hoechst and TO-PRO-3 images. TO-
998 PRO-3 objects that overlapped with Hoechst objects were counted as dead cells, while
999 Hoechst objects negative for TO-PRO-3 were counted as live cells.

1000 **Single cell RNA-sequencing alignment**

1001 *Gene expression library sequence alignment*

1002 A kallisto index was generated from the human transcriptome using the ENSEMBL cDNA
1003 reference (GRcH38). Introns were annotated using the GRCh38 version 112 genome
1004 annotation. The default k-mer size (k=31) was used in generation of the index. The gene
1005 expression library sequences were then pseudo-aligned to this index using kallisto-
1006 bustools.[93] After pseudo-alignment, barcodes were then corrected and filtered against the
1007 10X-v4 cell barcode whitelist.
1008

1009 *Knockdown Demultiplexing (sgRNA assignment)*

1010 A kallisto index was generated for the sgRNA library with a k-mer size of 15. The sgRNA
1011 enrichment PCR sequences were then pseudo-aligned to this index using kallisto
1012 bustools.[93] After pseudo-alignment, barcodes were corrected and filtered against the
1013 10X-v4 cell barcode whitelist. Cells were then assigned to guides using geomux
1014 (https://github.com/noamteyssier/geomux), which performs a hypergeometric test for
1015 each cell on its observed guide counts, then calculates a log2-odds ratio between the
1016 highest counts. Cells were assigned to their majority guide if their Benjamini-Hochberg
1017 corrected P-value was below 0.05, the log-odds ratio was above 1, and the total number
1018 of UMIs were greater than 5.
1019

1020 *Single-Cell Analysis*

Preprocessing

Cells were merged for the 10X sequence and the enrichment PCR by matching on cell-barcode and GEM library. Cells were filtered to only include those with a minimum count of 2000 and a minimum of 100 genes. 3000 of the most highly variable genes were selected with a minimum shared count of 10. Cells were further filtered to only include those with less and 8% and greater that 3% ribosomal gene content and less than 6.5% mitochondrial gene content. Cells were then normalized to a target sum of 1000 and log transformed. Principal component analysis was then performed using these highly variable genes. Clustering was performed using the Leiden algorithm, setting the resolution to 0.15. All single-cell filtering, transformation, and dimensionality reduction was performed using scanpy 1.10.3.

Differential Expression Analysis

Cells were grouped by knockdown, and GEM-library using ADPBulk (https://github.com/noamteyssier/adpbulk). Differential expression tests were performed using DESeq298 comparing each sgRNA knockdown against the non-targeting control sgRNAs.

Cluster overrepresentation analysis

We calculated Leiden cluster overrepresentation for each guide using a chi-square test for each guide/cluster in the dataset. Specifically, a chi-square test is performed for each knockdown group and Leiden cluster between each group distribution and each non-targeting control distribution. The p-values from this are then aggregated over the non-targeting controls using a geometric mean. Finally, these p-values are adjusted for multiple hypothesis testing using a Benjamini Hochberg correction. We performed this analysis using the open-source python module cshift (https://github.com/noamteyssier/cshift)

Knockdown Clustering Analysis and Gene Set Enrichment

Gene set enrichment analysis was performed using Enrichr and visualized using IDEA (https://github.com/noamteyssier/idea).

Software

GraphPad Prism v10.1.1; GraphPad Software; Boston, MA, USA

FlowJo analysis software v10.10.0; BD Life Sciences; Ashland, OR, USA

RStudio v2023.06.1+524 RStudio, PBC, Boston, MA, USA

Easy Electrophysiology software; v2.6; Cambridge, UK

Clampfit ;v10.7; Molecular Devices; San Jose, CA, USA

R packages used for presentation of data:

tidyverse, ggrepel, ggpubr, reshape2, dplyr, ggplot2, grid, WebGestaltR, extrafont, viridis, RColorBrewer, ggthemes, remotes, circlize, corrplot, Hmisc.

Python (3.12) packages used for processing and presentation of scRNA-seq data

scanpy	1.10.3
scikit-learn	1.5.2
scipy	1.14.1
adpbulk	0.1.4
anndata	0.10.9
pandas	2.2.3
matplotlib	3.9.2
seaborn	0.13.2
numpy	1.26.4

Statistics and reproducibility

No statistical methods were used to pre-determine sample sizes but our sample sizes are similar to those reported in previous publications.[23–25] No randomization of samples was used since treatment group of cells were generally derived from the same population of cells. Data collection and analysis were not performed blind to the conditions of the experiments. No data points were excluded from analysis. Data distribution was assumed to be normal but this was not formally tested.

Reporting summary

Further information on research design is available in the Nature Research Reporting Summary linked to this article.

Data availability

All screen datasets will be shared on the CRISPRbrain data commons (http://crisprbrain.org/) and will be shared upon request (associated with Figs. 2 and 4 and Extended Data Figs. 2). Single-cell RNA sequencing data will be deposited in NCBI GEO. There are no restrictions on data availability.

Code availability

The sgcount and crispr_screen bioinformatics pipelines for analysis of pooled screens are available on the Kampmann Lab website (https://kampmannlab.ucsf.edu/sgcount, https://kampmannlab.ucsf.edu/crisprscreen) and on Github (https://github.com/noamteyssier/sgcount, https://github.com/noamteyssier/crispr_screen). Analysis pipelines used to analyze CROP-seq data are open source and available on Github (ADPBulk-https://github.com/noamteyssier/adpbulk ; cshift-https://github.com/noamteyssier/cshift ; IDEA-https://github.com/noamteyssier/idea).

The CellProfiler pipelines will be made available on request to the corresponding authors (M.K.) and will also be submitted to the CellProfiler depository of published pipelines (https://cellprofiler.org/examples/ published_pipelines.html) upon publication.

Availability of biological materials

All materials can be requested from the corresponding author (M.K.) and will be made available without restrictions via a material transfer agreement.

Acknowledgements

We would like to thank Nick Page (UCSF) for contributions to preliminary experiments, the Weill Imaging Core and the Center for Advanced Light Microscopy, including Caroline Mrejen, So Yeon Kim, and Kari Herrington, for their technical support and microscopy instrumentation, the Laboratory for Cell Analysis and Sarah Elmes for use of FACS instruments.

We would like to thank Scott Martin, Ana Jovicic, and the Genentech Research and Early Development team (gRED) for their helpful discussions.

The authors would also like to thank Mor Alkaslasi, Olivia Teter and Avi Samelson for helpful comments and suggestions during the writing of this manuscript.

This research was funded by an award by the Alliance for Therapies in Neuroscience (ATN, Genentech and the University of California San Francisco) to M.K., an Alzheimer's Association Research Fellowship to S.C.B. (23AARF-1027616), a California Institute for Regenerative Medicine (CIRM) grant to J.Y.C. (EDUC2-12730), a Rainwater Charitable Foundation Tau Consortium Investigator award, a Ben Barres Early Career Acceleration award by the Chan Zuckerberg Initiative , and NIH/NINDS grant U54 NS123746 to M.K.

Sequencing was performed at the UCSF CAT, supported by UCSF PBBR, RRP IMIA, and NIH 1S10OD028511-01 grants.

Author contributions

Conceptualization of the CaMPARI2 based screen strategy was done by S.C.B, R.T, and M.K. CRISPRi screens and individual validation of screen hits were performed by S.C.B, V.G., E.M., and J.Y.C. sgRNA constructs for KD validation experiments were synthesized by S.C.B, V.G., J.Y.C, and L.Y. iNeuron-iAstrocyte coculture system was optimized by K.S. and S.C.B. CRISPR-RNP KOs in iPSC-neurons was performed by X. H., A.C, C.G.J., and C.E. Electrophysiology was performed by M.T. with input from J.H. CRISPR screen analysis was performed by S.C.B. with an analysis pipeline developed by N.T.. CROP-seq library preparation, cell preparation, and analysis was performed by S.C.B. and analysis was advised by N.T.. S.C.B, V.G., and M.T. created the figures, with input from all authors. S.C.B and M.K wrote the manuscript with input from all authors. All authors reviewed and approved the final manuscript.

Competing interests

M.K. is a co-scientific founder of Montara Therapeutics and serves on the Scientific Advisory Boards of Engine Biosciences, Casma Therapeutics, Alector, and Montara Therapeutics, and is an advisor to Modulo Bio and Recursion Therapeutics. M.K. is an inventor on US Patent 11,254,933 related to CRISPRi and CRISPRa screening, and on a US Patent application on *in vivo* screening methods. M.T., X.H., A.C, C.G.J., C.E., and J.H. are employees of Genentech. S.C.B is currently employed at the Arc Institute (Palo Alto, CA).

References

1. Scala, F. *et al.* Phenotypic variation of transcriptomic cell types in mouse motor cortex. *Nature* **598**, 144–150 (2021).
2. BRAIN Initiative Cell Census Network (BICCN). A multimodal cell census and atlas of the mammalian primary motor cortex. *Nature* **598**, 86–102 (2021).
3. Ecker, J. R. *et al.* The BRAIN Initiative Cell Census Consortium: Lessons Learned toward Generating a Comprehensive Brain Cell Atlas. *Neuron* **96**, 542–557 (2017).
4. Yuste, R. *et al.* A community-based transcriptomics classification and nomenclature of neocortical cell types. *Nat Neurosci* **23**, 1456–1468 (2020).
5. Jorstad, N. L. *et al.* Transcriptomic cytoarchitecture reveals principles of human neocortex organization. *Science* **382**, eadf6812 (2023).
6. Kandel, E. R. The molecular biology of memory storage: a dialogue between genes and synapses. *Science* **294**, 1030–1038 (2001).
7. West, A. E. & Greenberg, M. E. Neuronal Activity–Regulated Gene Transcription in Synapse Development and Cognitive Function. *Cold Spring Harb Perspect Biol* **3**, a005744 (2011).
8. Fang, R. *et al.* Conservation and divergence of cortical cell organization in human and mouse revealed by MERFISH. *Science* **377**, 56–62 (2022).
9. Yao, Z. *et al.* A high-resolution transcriptomic and spatial atlas of cell types in the whole mouse brain. *Nature* **624**, 317–332 (2023).
10. Jin, K. *et al.* Cell-type specific molecular signatures of aging revealed in a brain-wide transcriptomic cell-type atlas. 2023.07.26.550355 Preprint at https://doi.org/10.1101/2023.07.26.550355 (2023).
11. Camunas-Soler, J. *et al.* Patch-Seq Links Single-Cell Transcriptomes to Human Islet Dysfunction in Diabetes. *Cell Metabolism* **31**, 1017-1031.e4 (2020).
12. International League Against Epilepsy Consortium on Complex Epilepsies. GWAS meta-analysis of over 29,000 people with epilepsy identifies 26 risk loci and subtype-specific genetic architecture. *Nat Genet* **55**, 1471–1482 (2023).
13. Guerrini, R., Balestrini, S., Wirrell, E. C. & Walker, M. C. Monogenic Epilepsies. *Neurology* **97**, 817–831 (2021).
14. Kunkle, B. W. *et al.* Genetic meta-analysis of diagnosed Alzheimer's disease identifies new risk loci and implicates Aβ, tau, immunity and lipid processing. *Nat Genet* **51**, 414–430 (2019).
15. Satterstrom, F. K. *et al.* Large-Scale Exome Sequencing Study Implicates Both Developmental and Functional Changes in the Neurobiology of Autism. *Cell* **180**, 568-584.e23 (2020).
16. Zhang, Y. & Looger, L. L. Fast and sensitive GCaMP calcium indicators for neuronal imaging. *J Physiol* (2023) doi:10.1113/JP283832.
17. Knöpfel, T. & Song, C. Optical voltage imaging in neurons: moving from technology development to practical tool. *Nat Rev Neurosci* **20**, 719–727 (2019).
18. Liu, P. & Miller, E. W. Electrophysiology, Unplugged: Imaging Membrane Potential with Fluorescent Indicators. *Acc Chem Res* **53**, 11–19 (2020).
19. Deisseroth, K. Optogenetics. *Nat Methods* **8**, 26–29 (2011).
20. Kim, C. K., Adhikari, A. & Deisseroth, K. Integration of optogenetics with complementary methodologies in systems neuroscience. *Nat Rev Neurosci* **18**, 222–235 (2017).

21. Boivin, B. *et al.* A multiparametric activity profiling platform for neuron disease phenotyping and drug screening. *Mol Biol Cell* **33**, ar54 (2022).
22. Gilbert, L. A. *et al.* Genome-Scale CRISPR-Mediated Control of Gene Repression and Activation. *Cell* **159**, 647–661 (2014).
23. Tian, R. *et al.* CRISPR Interference-Based Platform for Multimodal Genetic Screens in Human iPSC-Derived Neurons. *Neuron* **104**, 239-255.e12 (2019).
24. Tian, R. *et al.* Genome-wide CRISPRi/a screens in human neurons link lysosomal failure to ferroptosis. *Nat Neurosci* **24**, 1020–1034 (2021).
25. Dräger, N. M. *et al.* A CRISPRi/a platform in human iPSC-derived microglia uncovers regulators of disease states. *Nat Neurosci* **25**, 1149–1162 (2022).
26. Leng, K. *et al.* CRISPRi screens in human iPSC-derived astrocytes elucidate regulators of distinct inflammatory reactive states. *Nat Neurosci* (2022) doi:10.1038/s41593-022-01180-9.
27. Li, E. *et al.* CRISPRi-based screens in iAssembloids to elucidate neuron-glia interactions. *Neuron* **0**, (2025).
28. Samelson, A. J. *et al.* CRISPR screens in iPSC-derived neurons reveal principles of tau proteostasis. 2023.06.16.545386 Preprint at https://doi.org/10.1101/2023.06.16.545386 (2023).
29. Ebner, C. *et al.* Optically Induced Calcium-Dependent Gene Activation and Labeling of Active Neurons Using CaMPARI and Cal-Light. *Front Synaptic Neurosci* **11**, 16 (2019).
30. Trojanowski, N. F., Bottorff, J. & Turrigiano, G. G. Activity labeling in vivo using CaMPARI2 reveals intrinsic and synaptic differences between neurons with high and low firing rate set points. *Neuron* **109**, 663-676.e5 (2021).
31. Zolnik, T. A. *et al.* All-optical functional synaptic connectivity mapping in acute brain slices using the calcium integrator CaMPARI: CaMPARI for all-optical functional connectivity mapping *ex vivo*. *J Physiol* **595**, 1465–1477 (2017).
32. Moeyaert, B. *et al.* Improved methods for marking active neuron populations. *Nat Commun* **9**, 4440 (2018).
33. Carreras-Sureda, A. *et al.* The ER stress sensor IRE1 interacts with STIM1 to promote store-operated calcium entry, T cell activation, and muscular differentiation. *Cell Rep* **42**, 113540 (2023).
34. Perdigão, C. *et al.* Intracellular Trafficking Mechanisms of Synaptic Dysfunction in Alzheimer's Disease. *Front Cell Neurosci* **14**, 72 (2020).
35. Zoghbi, H. Y. & Bear, M. F. Synaptic Dysfunction in Neurodevelopmental Disorders Associated with Autism and Intellectual Disabilities. *Cold Spring Harbor Perspectives in Biology* **4**, a009886–a009886 (2012).
36. Hoover, B. R. *et al.* Tau mislocalization to dendritic spines mediates synaptic dysfunction independently of neurodegeneration. *Neuron* **68**, 1067–1081 (2010).
37. Li, K. *et al.* Synaptic Dysfunction in Alzheimer's Disease: Aβ, Tau, and Epigenetic Alterations. *Mol Neurobiol* **55**, 3021–3032 (2018).
38. Keller, R., Basta, R., Salerno, L. & Elia, M. Autism, epilepsy, and synaptopathies: a not rare association. *Neurol Sci* **38**, 1353–1361 (2017).
39. Vossel, K. A. *et al.* Seizures and epileptiform activity in the early stages of Alzheimer disease. *JAMA Neurol* **70**, 1158–1166 (2013).

1241 40. Vossel, K. A. *et al.* Incidence and impact of subclinical epileptiform activity in
1242 Alzheimer's disease. *Annals of Neurology* **80**, 858–870 (2016).
1243 41. Beagle, A. J. *et al.* Relative Incidence of Seizures and Myoclonus in Alzheimer's
1244 Disease, Dementia with Lewy Bodies, and Frontotemporal Dementia. *J Alzheimers*
1245 *Dis* **60**, 211–223 (2017).
1246 42. Palop, J. J. & Mucke, L. Network abnormalities and interneuron dysfunction in
1247 Alzheimer disease. *Nat Rev Neurosci* **17**, 777–792 (2016).
1248 43. Zimmern, V., Minassian, B. & Korff, C. A Review of Targeted Therapies for
1249 Monogenic Epilepsy Syndromes. *Front Neurol* **13**, 829116 (2022).
1250 44. Nagy, T. & Kampmann, M. CRISPulator: a discrete simulation tool for pooled genetic
1251 screens. *BMC Bioinformatics* **18**, (2017).
1252 45. Wang, J., Vasaikar, S., Shi, Z., Greer, M. & Zhang, B. WebGestalt 2017: a more
1253 comprehensive, powerful, flexible and interactive gene set enrichment analysis
1254 toolkit. *Nucleic Acids Research* **45**, W130–W137 (2017).
1255 46. Krukowski, K. *et al.* Small molecule cognitive enhancer reverses age-related
1256 memory decline in mice. *eLife* **9**, e62048 (2020).
1257 47. Costa-Mattioli, M. *et al.* eIF2alpha phosphorylation bidirectionally regulates the
1258 switch from short- to long-term synaptic plasticity and memory. *Cell* **129**, 195–206
1259 (2007).
1260 48. Sharma, V. *et al.* eIF2α controls memory consolidation via excitatory and
1261 somatostatin neurons. *Nature* **586**, 412–416 (2020).
1262 49. Larsson, M., Agalave, N., Watanabe, M. & Svensson, C. I. Distribution of
1263 transmembrane AMPA receptor regulatory protein (TARP) isoforms in the rat spinal
1264 cord. *Neuroscience* **248**, 180–193 (2013).
1265 50. Yamasaki, M. *et al.* TARP γ-2 and γ-8 Differentially Control AMPAR Density Across
1266 Schaffer Collateral/Commissural Synapses in the Hippocampal CA1 Area. *J*
1267 *Neurosci* **36**, 4296–4312 (2016).
1268 51. Bats, C., Groc, L. & Choquet, D. The Interaction between Stargazin and PSD-95
1269 Regulates AMPA Receptor Surface Trafficking. *Neuron* **53**, 719–734 (2007).
1270 52. Chen, L. *et al.* Stargazin regulates synaptic targeting of AMPA receptors by two
1271 distinct mechanisms. *Nature* **408**, 936–943 (2000).
1272 53. Adotevi, N. K. & Leitch, B. Alterations in AMPA receptor subunit expression in
1273 cortical inhibitory interneurons in the epileptic stargazer mutant mouse.
1274 *Neuroscience* **339**, 124–138 (2016).
1275 54. Jackson, A. C. & Nicoll, R. A. The Expanding Social Network of Ionotropic
1276 Glutamate Receptors: TARPs and Other Transmembrane Auxiliary Subunits.
1277 *Neuron* **70**, 178–199 (2011).
1278 55. Oguro, K. *et al.* Knockdown of AMPA Receptor GluR2 Expression Causes Delayed
1279 Neurodegeneration and Increases Damage by Sublethal Ischemia in Hippocampal
1280 CA1 and CA3 Neurons. *J Neurosci* **19**, 9218–9227 (1999).
1281 56. Friedman, L. K. Selective reduction of GluR2 protein in adult hippocampal CA3
1282 neurons following status epilepticus but prior to cell loss. *Hippocampus* **8**, 511–525
1283 (1998).
1284 57. Smeets, C. J. L. M., Ma, K. Y., Fisher, S. E. & Verbeek, D. S. Cerebellar
1285 developmental deficits underlie neurodegenerative disorder spinocerebellar ataxia
1286 type 23. *Brain Pathol* **31**, 239–252 (2020).

58. Parsons, R. Discovery of the PTEN Tumor Suppressor and Its Connection to the PI3K and AKT Oncogenes. *Cold Spring Harb Perspect Med* **10**, a036129 (2020).
59. Wang, L., Lu, G. & Shen, H.-M. The Long and the Short of PTEN in the Regulation of Mitophagy. *Frontiers in Cell and Developmental Biology* **8**, (2020).
60. Williams, M. R., DeSpenza, T., Li, M., Gulledge, A. T. & Luikart, B. W. Hyperactivity of Newborn Pten Knock-out Neurons Results from Increased Excitatory Synaptic Drive. *J Neurosci* **35**, 943–959 (2015).
61. Azarnia Tehran, D. *et al.* Selective endocytosis of Ca2+-permeable AMPARs by the Alzheimer's disease risk factor CALM bidirectionally controls synaptic plasticity. *Science Advances* **8**, eabl5032 (2022).
62. Brunet, M., Vargas, C., Larrieu, D., Torrisani, J. & Dufresne, M. E3 Ubiquitin Ligase TRIP12: Regulation, Structure, and Physiopathological Functions. *Int J Mol Sci* **21**, 8515 (2020).
63. Gudjonsson, T. *et al.* TRIP12 and UBR5 Suppress Spreading of Chromatin Ubiquitylation at Damaged Chromosomes. *Cell* **150**, 697–709 (2012).
64. Chauhan, A. S., Jhujh, S. S. & Stewart, G. S. E3 ligases: a ubiquitous link between DNA repair, DNA replication and human disease. *Biochem J* **481**, 923–944 (2024).
65. García-Cabrero, A. M. *et al.* Hyperexcitability and epileptic seizures in a model of frontotemporal dementia. *Neurobiol Dis* **58**, 200–208 (2013).
66. Wainger, B. J. *et al.* Intrinsic Membrane Hyperexcitability of Amyotrophic Lateral Sclerosis Patient-Derived Motor Neurons. *Cell Reports* **7**, 1–11 (2014).
67. Gomez-Murcia, V. *et al.* Hyperexcitability and seizures in the THY-Tau22 mouse model of tauopathy. *Neurobiol Aging* **94**, 265–270 (2020).
68. Telias, M. Molecular Mechanisms of Synaptic Dysregulation in Fragile X Syndrome and Autism Spectrum Disorders. *Front Mol Neurosci* **12**, 51 (2019).
69. Trimmer, J. S. Subcellular localization of K+ channels in mammalian brain neurons: remarkable precision in the midst of extraordinary complexity. *Neuron* **85**, 238–256 (2015).
70. Yang, B., Desai, R. & Kaczmarek, L. K. Slack and Slick KNa Channels Regulate the Accuracy of Timing of Auditory Neurons. *J Neurosci* **27**, 2617–2627 (2007).
71. Kim, G. E. & Kaczmarek, L. K. Emerging role of the KCNT1 Slack channel in intellectual disability. *Front Cell Neurosci* **8**, 209 (2014).
72. Møller, R. S. *et al.* Mutations in KCNT1 cause a spectrum of focal epilepsies. *Epilepsia* **56**, e114–e120 (2015).
73. Gong, P., Jiao, X., Yu, D. & Yang, Z. Case Report: Causative De novo Variants of KCNT2 for Developmental and Epileptic Encephalopathy. *Front Genet* **12**, 649556 (2021).
74. Ambrosino, P. *et al.* De novo gain-of-function variants in KCNT2 as a novel cause of developmental and epileptic encephalopathy. *Ann Neurol* **83**, 1198–1204 (2018).
75. Dreyling, M. H. *et al.* The t(10;11)(p13;q14) in the U937 cell line results in the fusion of the AF10 gene and CALM, encoding a new member of the AP-3 clathrin assembly protein family. *Proc Natl Acad Sci U S A* **93**, 4804–4809 (1996).
76. Tebar, F., Bohlander, S. K. & Sorkin, A. Clathrin Assembly Lymphoid Myeloid Leukemia (CALM) Protein: Localization in Endocytic-coated Pits, Interactions with Clathrin, and the Impact of Overexpression on Clathrin-mediated Traffic. *Mol Biol Cell* **10**, 2687–2702 (1999).

77. Harold, D. *et al.* Genome-wide association study identifies variants at CLU and PICALM associated with Alzheimer's disease. *Nat Genet* **41**, 1088–1093 (2009).
78. Bellenguez, C. *et al.* New insights into the genetic etiology of Alzheimer's disease and related dementias. *Nat Genet* **54**, 412–436 (2022).
79. Jun, G. *et al.* Meta-Analysis confirms CR1, CLU, and PICALM as Alzheimer's disease risk loci and reveals interactions with APOE genotypes. *Arch Neurol* **67**, 1473–1484 (2010).
80. Lambert, J.-C. *et al.* Evidence of the association of BIN1 and PICALM with the AD risk in contrasting European populations. *Neurobiology of Aging* **32**, 756.e11-756.e15 (2011).
81. Moreau, K. *et al.* PICALM modulates autophagy activity and tau accumulation. *Nat Commun* **5**, 4998 (2014).
82. Sanchez, M. I., Nguyen, Q.-A., Wang, W., Soltesz, I. & Ting, A. Y. Transcriptional readout of neuronal activity via an engineered Ca2+-activated protease. *PNAS* **117**, 33186–33196 (2020).
83. Kim, C. K. *et al.* A Molecular Calcium Integrator Reveals a Striatal Cell Type Driving Aversion. *Cell* **183**, 2003-2019.e16 (2020).
84. Bardy, C. *et al.* Neuronal medium that supports basic synaptic functions and activity of human neurons in vitro. *Proc Natl Acad Sci USA* **112**, E2725–E2734 (2015).
85. Satir, T. M. *et al.* Accelerated neuronal and synaptic maturation by BrainPhys medium increases Aβ secretion and alters Aβ peptide ratios from iPSC-derived cortical neurons. *Sci Rep* **10**, 601 (2020).
86. Shih, P.-Y. *et al.* Development of a fully human assay combining NGN2-inducible neurons co-cultured with iPSC-derived astrocytes amenable for electrophysiological studies. *Stem Cell Research* **54**, 102386 (2021).
87. Meijer, M. *et al.* A Single-Cell Model for Synaptic Transmission and Plasticity in Human iPSC-Derived Neurons. *Cell Reports* **27**, 2199-2211.e6 (2019).
88. Nehme, R. *et al.* Combining NGN2 Programming with Developmental Patterning Generates Human Excitatory Neurons with NMDAR-Mediated Synaptic Transmission. *Cell Reports* **23**, 2509–2523 (2018).
89. Shan, X. *et al.* Fully defined NGN2 neuron protocol reveals diverse signatures of neuronal maturation. *Cell Rep Methods* **4**, 100858 (2024).
90. Piñero, J. *et al.* The DisGeNET knowledge platform for disease genomics: 2019 update. *Nucleic Acids Research* **48**, D845–D855 (2020).
91. Horlbeck, M. A. *et al.* Compact and highly active next-generation libraries for CRISPR-mediated gene repression and activation. *eLife* **5**, e19760 (2016).
92. Li, W. *et al.* MAGeCK enables robust identification of essential genes from genome-scale CRISPR/Cas9 knockout screens. *Genome Biol* **15**, 554 (2014).
93. Melsted, P. *et al.* Modular, efficient and constant-memory single-cell RNA-seq preprocessing. *Nat Biotechnol* **39**, 813–818 (2021).

Figures

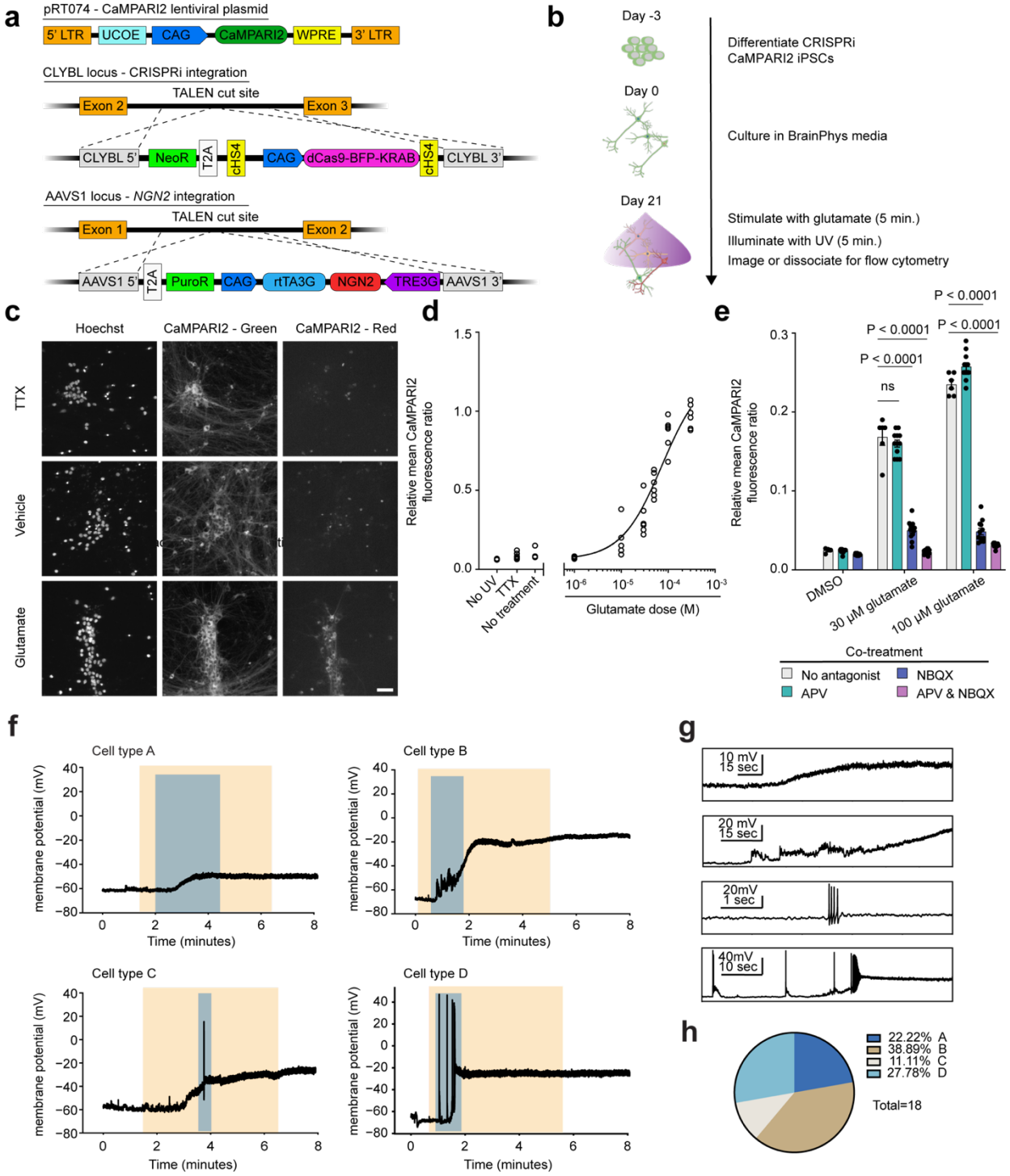
a
pRT074 - CaMPARI2 lentiviral plasmid
5' LTR
UCOE
CAG
CaMPARI2
WPRE
3' LTR
CLYBL locus - CRISPRi integration
TALEN cut site
Exon 2
Exon 3
CLYBL 5'
NeoR
T2A
cHS4
CAG
dCas9-BFP-KRAB
cHS4
CLYBL 3'
AAVS1 locus - NGN2 integration
TALEN cut site
Exon 1
Exon 2
AAVS1 5'
T2A
PuroR
CAG
rtTA3G
NGN2
TRE3G
AAVS1 3'
b
Day -3
Differentiate CRISPRi CaMPARI2 iPSCs
Day 0
Culture in BrainPhys media
Day 21
Stimulate with glutamate (5 min.)
Illuminate with UV (5 min.)
Image or dissociate for flow cytometry
c
Hoechst
CaMPARI2 - Green
CaMPARI2 - Red
TTX
Vehicle
Glutamate
d
Relative mean CaMPARI2 fluorescence ratio
No UV
TTX
No treatment
Glutamate dose (M)
e
Relative mean CaMPARI2 fluorescence ratio
P < 0.0001
ns
DMSO
30 μM glutamate
100 μM glutamate
Co-treatment
No antagonist
APV
NBQX
APV & NBQX
f
Cell type A
Cell type B
Cell type C
Cell type D
membrane potential (mV)
Time (minutes)
g
10 mV
15 sec
20 mV
15 sec
20mV
1 sec
40mV
10 sec
h
22.22% A
38.89% B
11.11% C
27.78% D
Total=18

Figure 1. CaMPARI2 captures glutamate receptor activation in iPSC-derived glutamatergic neurons.

(a) Strategy for generating CRISPRi-NGN2-CaMPARI2 iPSC line: NGN2 and dCAS9-KRAB was stably integrated into the AAVS1 and CLYBL loci, respectively, as described previously.17 CAG promoter-driven CaMPARI2 was randomly inserted into the genome via lentiviral integration. UCOE: Ubiquitous Chromatin Opening Element, WPRE: Woodchuck Hepatitis Virus Posttranscriptional Regulatory Element.

(b) Experimental workflow of CaMPARI2 photoconversion assay in glutamatergic NGN2 neurons.

(c) Representative fluorescence micrographs of iPSC-neurons expressing CaMPARI2 following incubation with 1.5 μM tetrodotoxin (TTX), vehicle (0.1% DMSO), or 30 μM glutamate for 5 minutes and illumination with 405 nm light. Nuclei were stained with Hoechst 33342. Unconverted CaMPARI2 persists in the soma and neurites, and converted CaMPARI2 is only observed with high signal after incubation with 30 μM glutamate. Merged micrographs show colocalization of nuclei (blue), CaMPARI2 (green), and converted CaMPARI2 (magenta). Scale bar is 20 μm.

(d) CaMPARI2 neurons respond to glutamate in a dose-dependent manner. N = 6 independent culture wells per measurement. “No UV”, TTX (1.5 μM), and “no treatment” conditions did not contain glutamate.

(e) Co-incubation of glutamate with AMPA receptor (10 μM NBQX), but not NMDA receptor (50 μM APV), antagonists attenuate CaMPARI2 photoconversion, suggesting that AMPA receptor activation is the primary mechanism of calcium influx. N = 6 independent culture wells per measurement. Unpaired t-test, * = P <0.0001. Error bars are SEM.

(f) Representative current clamp recordings from four different cell types. The orange shaded area indicates the 5-minute window when 30 μM glutamate was applied to the recording chamber. The blue shaded area highlights the zoomed-in view shown in (g) for each trace.

(g) From top to bottom, a zoomed-in view of the blue shaded areas from (f) for Cell types A to D.

(h) Percentage of each cell type from recorded iNeurons. N = 18 neurons.

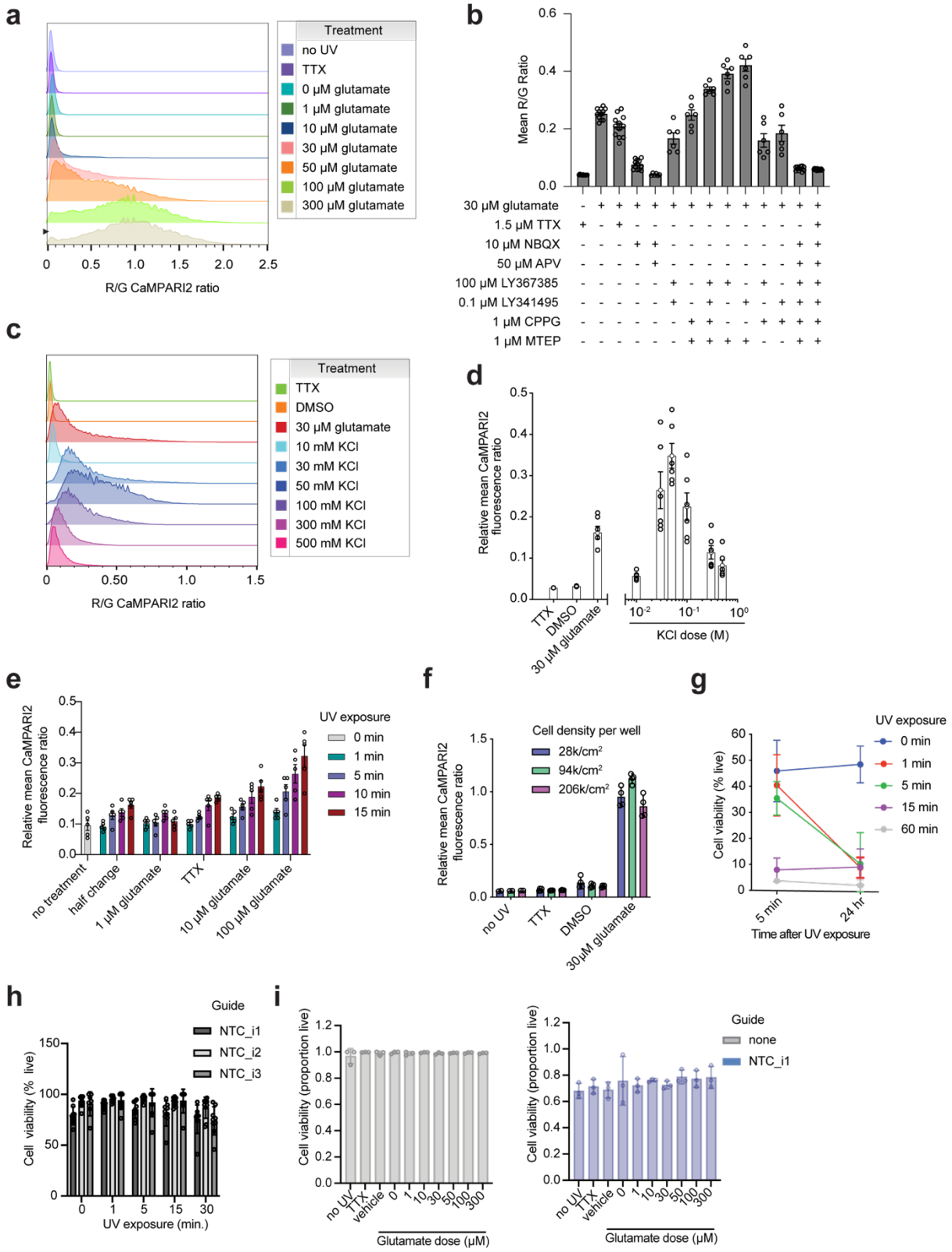

1408
1409
1410

1411 **Extended Data Figure 1. CaMPARI2 reliably conveys AMPAR activation at the**
1412 **synapse without significant UV toxicity.**
1413 (a) CaMPARI2 dose response to glutamate. CaMPARI2 iNeurons were treated with
1414 TTX or various concentrations of glutamate (0, 1, 10, 30, 60, or 100 μM) and illuminated
1415 with UV to measure photoconversion of CaMPARI2. Photoconversion increased in a
1416 dose-dependent manner.
1417 (b) CaMPARI2 response to glutamate with co-treatment of GluR antagonists and TTX.
1418 CaMPARI2 activation is reduced to baseline (neurons treated with 1.5 μM TTX) when
1419 treated with APV and NBQX. Activation is not fully reduced to baseline with a full spectrum
1420 cocktail of mGluR antagonists, but is still lower than glutamate treatment alone. N = 6
1421 independent culture wells.
1422 (c) CaMPARI2 dose response to KCl. CaMPARI2 iNeurons were treated with TTX, 30
1423 μM glutamate, 0.1% DMSO or various concentrations of KCl (10, 30, 50, 100, 300, 500
1424 mM) and illuminated with UV to measure photoconversion of CaMPARI2.
1425 Photoconversion increased in a dose-dependent manner to a peak at 50 mM, where a
1426 decline in photoconversion was observed at higher concentrations of KCl.
1427 (d) Quantification of CaMPARI2 red/green fluorescence ratio from (b). A non-linear fit
1428 could not be established, however the 50 mM KCl treatment was selected for later
1429 experiments due to the high conversion and range of response. N = 6 independent culture
1430 wells.
1431 (e) CaMPARI photoconversion in response to various UV durations. CaMPARI2
1432 iNeurons were treated with TTX or various concentrations of glutamate (0, 1, 10, or 100
1433 μM) and illuminated with UV for various durations of time (0, 1, 5, 10, or 15 min). After
1434 illumination, cells were dissociated for flow cytometry and analyzed. N = 5 independent
1435 culture wells.
1436 (f) Measuring effect of cell density on CaMPARI photoconversion. Significant
1437 deviations from optimal plating conditions had no significant effects on photoconversion
1438 upon TTX, vehicle, or glutamate treatment. N=4 independent culture wells.
1439 (g) Measuring UV toxicity in CaMPARI iNeurons. iNeurons were illuminated with UV
1440 for 0, 1, 5, 15, or 60 minutes and stained with Trypan Blue or TOPRO viability stain 5
1441 minutes or 24 hours later to assess UV toxicity. N = 3 independent culture wells.
1442 (h) Measuring UV toxicity in CaMPARI iNeurons. CaMPARI iNeurons were illuminated
1443 with UV for 0, 1, 5, 15, or 30 minutes. Viability staining with TO-PRO-3 shows the
1444 proportion of viable cells after UV exposure. N = 9 independent culture wells.
1445 (i) Measuring glutamate toxicity. CaMPARI iNeurons were treated with 0, 1, 3, 10, 30,
1446 50, 100 μM of glutamate for 5 minutes and UV illuminated for 5 minutes. TO-PRO-3
1447 staining was performed to measure acute glutamate treatment toxicity. N = 3 independent
1448 culture wells.
1449
1450
1451
1452

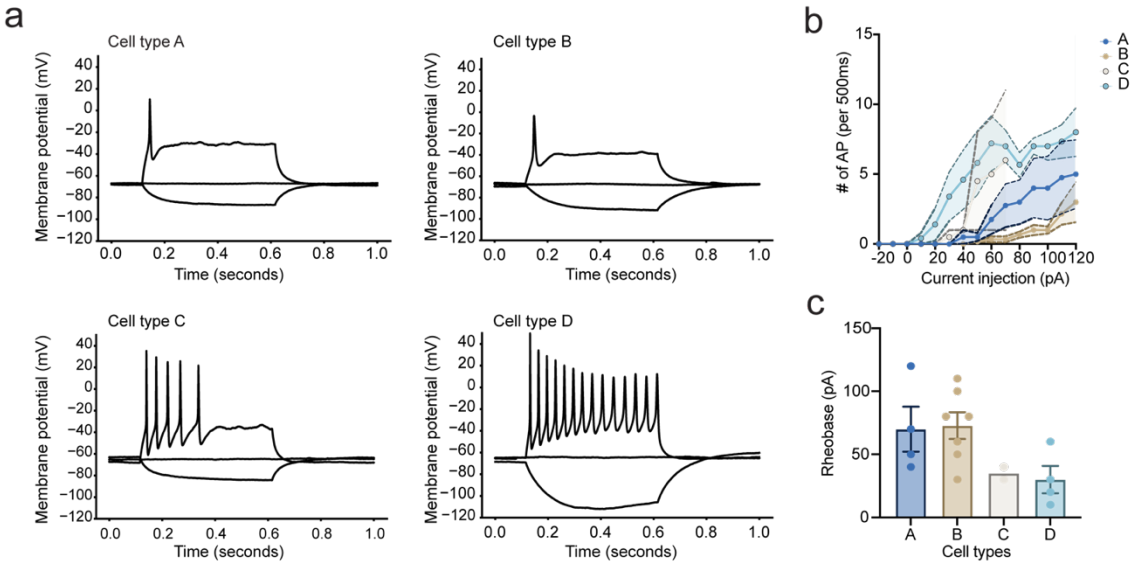

Extended Data Figure 2. iNeurons have heterogeneous responses to glutamate stimulation

(a) Representative voltage responses from the current-spike output recordings of the corresponding iNeurons in Figure 1f-h.

(b) Current-spike output relationships for all recorded iNeurons in Figure 1f-h. N = 2-7 independent neurons per cell type, 18 neurons total. Shaded error bars are S.E.M.

(c) Rheobase values for all recorded iNeurons in Figure 1f-h. N = 2-7 independent neurons per cell type, 18 neurons total. One-way ANOVA, p = 0.05. Error bars are S.E.M.

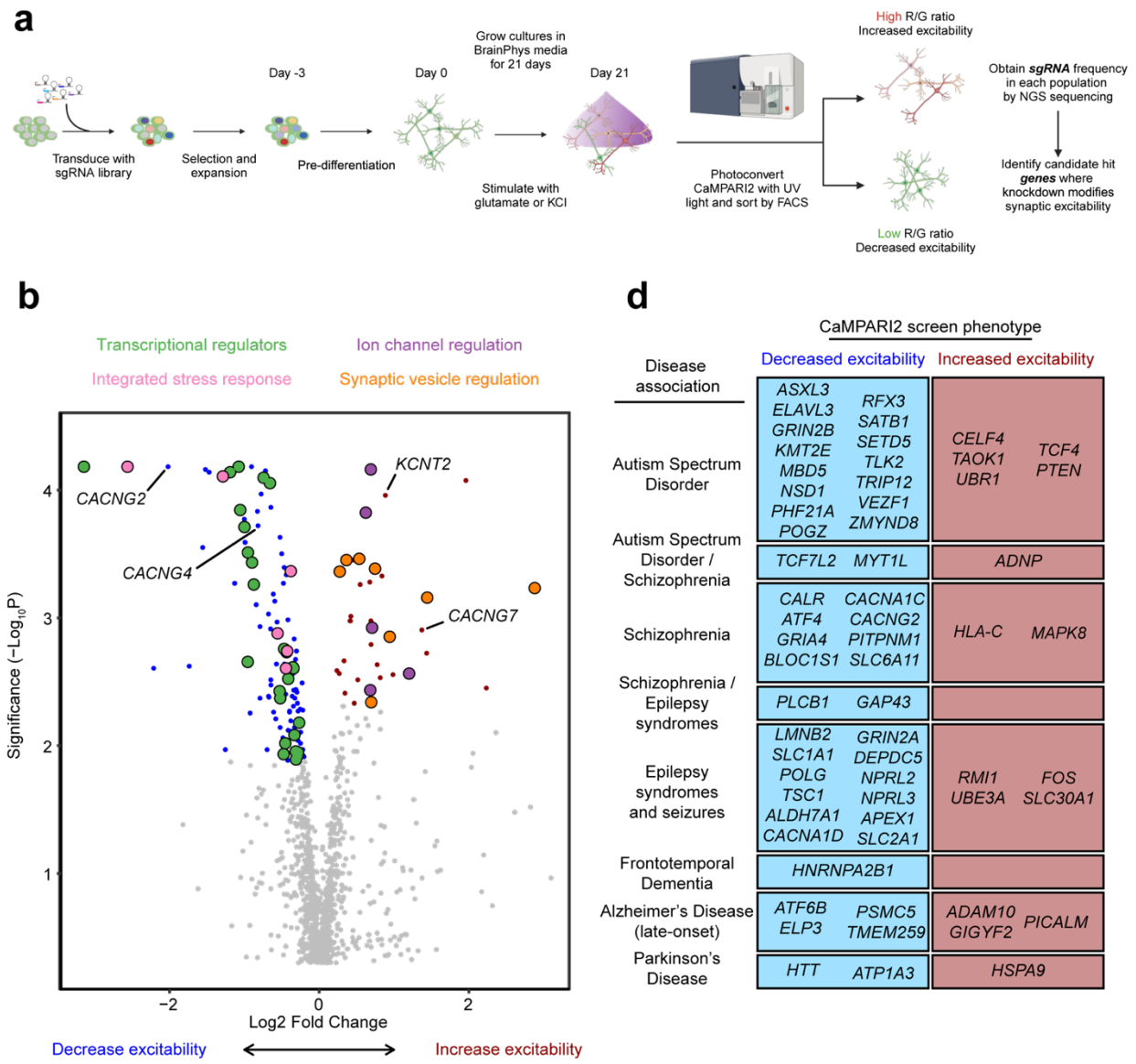
a
Transduce with sgRNA library
Selection and expansion
Day -3
Pre-differentiation
Day 0
Grow cultures in BrainPhys media for 21 days
Stimulate with glutamate or KCl
Day 21
Photoconvert CaMPARI2 with UV light and sort by FACS
High R/G ratio
Increased excitability
Low R/G ratio
Decreased excitability
Obtain sgRNA frequency in each population by NGS sequencing
Identify candidate hit genes where knockdown modifies synaptic excitability
b
Transcriptional regulators
Ion channel regulation
Integrated stress response
Synaptic vesicle regulation
CACNG2
CACNG4
KCNT2
CACNG7
Significance (−Log10P)
Log2 Fold Change
Decrease excitability
Increase excitability
d
CaMPARI2 screen phenotype
Disease association
Decreased excitability
Increased excitability
Autism Spectrum Disorder
ASXL3 ELAVL3 GRIN2B KMT2E MBD5 NSD1 PHF21A POGZ RFX3 SATB1 SETD5 TLK2 TRIP12 VEZF1 ZMYND8
CELF4 TAOK1 UBR1 TCF4 PTEN
Autism Spectrum Disorder / Schizophrenia
TCF7L2 MYT1L
ADNP
Schizophrenia
CALR ATF4 GRIA4 BLOC1S1 CACNA1C CACNG2 PITPNM1 SLC6A11
HLA-C MAPK8
Schizophrenia / Epilepsy syndromes
PLCB1 GAP43
Epilepsy syndromes and seizures
LMNB2 SLC1A1 POLG TSC1 ALDH7A1 CACNA1D GRIN2A DEPDC5 NPRL2 NPRL3 APEX1 SLC2A1
RMI1 UBE3A FOS SLC30A1
Frontotemporal Dementia
HNRNPA2B1
Alzheimer's Disease (late-onset)
ATF6B ELP3 PSMC5 TMEM259
ADAM10 GIGYF2 PICALM
Parkinson's Disease
HTT ATP1A3
HSPA9
c
Transcription regulator activity
Chromatin
Sequence−specific DNA binding
Cellular response to amino acid starvation
Lipid droplet
NF−kappaB binding
Activation of cysteine−type endopeptidase activity
Hits decreasing CaMPARI ratio
Enrichment Ratio
Regulation of protein localization to membrane
Negative regulation of ion transmembrane transport
Protein serine/threonine kinase activator activity
Clathrin coat assembly
Response to corticosterone
Hits increasing CaMPARI ratio
Enrichment Ratio

Figure 2. CRISPR interference (CRISPRi) screening with CaMPARI2 reveals genetic modifiers of neuronal excitability in iPSC derived neurons.

(a) Screening strategy using CaMPARI2 as readout for neuronal excitability. CRISPRi iPSC expressing CaMPARI2 were transduced with a lentiviral sgRNA library focused on genes annotated for neuronal activity, neurodegenerative disease, or neurodevelopmental disorders (7449 sgRNA constructs targeting 1343 genes). Exposure to puromycin selects for iPSCs successfully transduced with sgRNA construct. iPSCs were then differentiated into neurons via overexpression of NGN2 and cultured for 21 days. Neurons were then incubated with 30 μM glutamate for five minutes, illuminated with UV light for five minutes, and then separated by FACS into high and low red/green fluorescence ratio populations. Frequency of neurons expressing sgRNAs were determined by next-generation sequencing for high and low red/green ratio neuronal populations and hit genes were identified.

(b) Volcano plot summarizing the effect of knockdowns on CaMPARI phenotypes and the determine statistical significance for targeted genes (Mann-Whitney U test). Dashed lines indicate a false-discovery rate (FDR) cutoff of 0.05, based on the phenotype score for genes calculated from 5 targeting sgRNAs. Red and blue points indicate hit genes where knockdown increases and decreases CaMPARI2 red/green fluorescence ratio, respectively, in response to glutamate stimulation. Grey points indicate non-hits. Large colored dots indicate hit genes that were found in the enriched GO terms in (d).

(c) Disease-associated genes that influenced excitability in the CaMPARI2 screen.

(d) Over-representation analysis (ORA) using Webgestalt indicates gene ontology (GO) annotation terms that describe genes enriched in the low (blue) and high (red) CaMPARI2 ratio from the screening library.

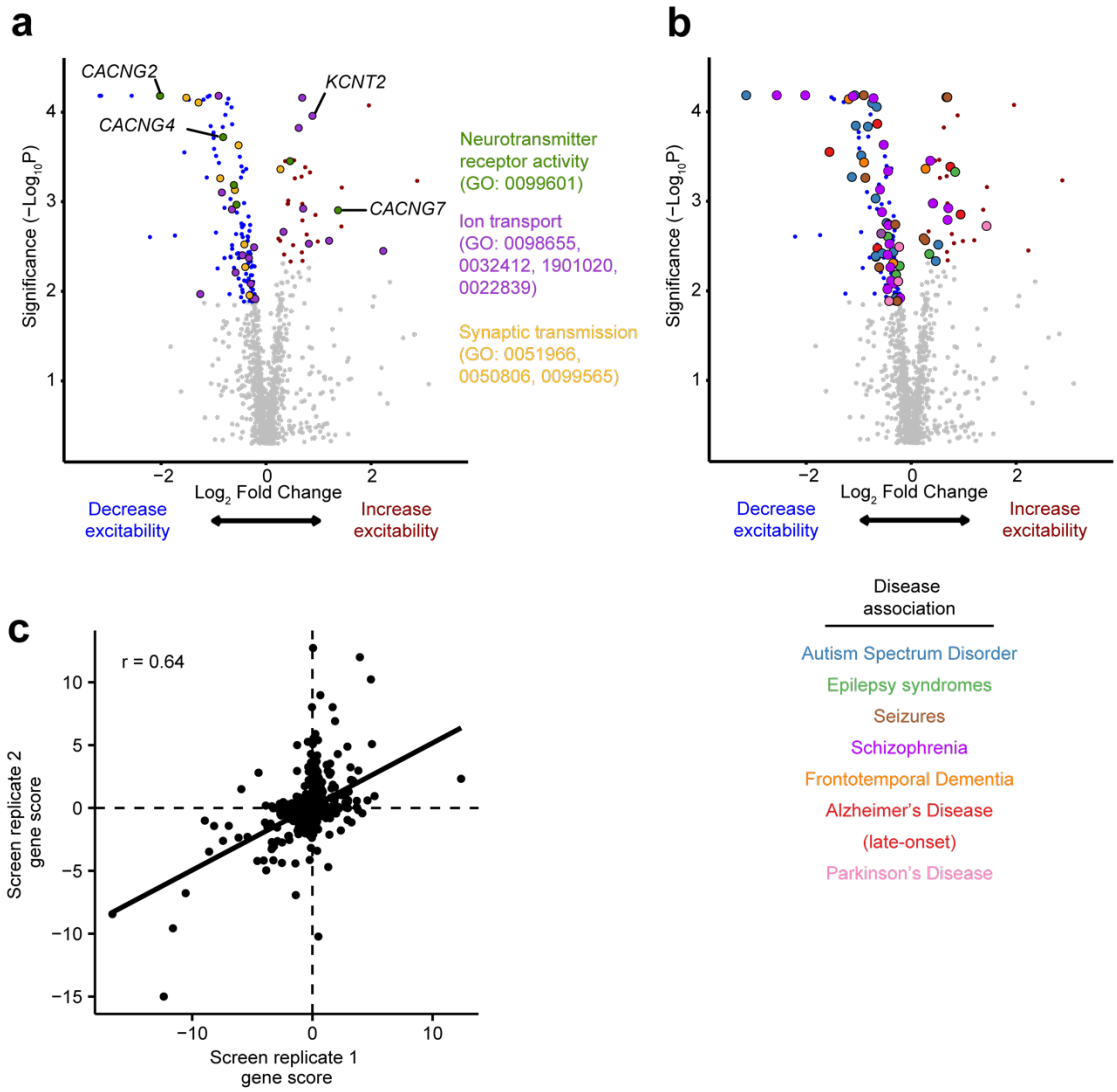
a
CACNG2
KCNT2
CACNG4
CACNG7
Neurotransmitter receptor activity (GO: 0099601)
Ion transport (GO: 0098655, 0032412, 1901020, 0022839)
Synaptic transmission (GO: 0051966, 0050806, 0099565)
Significance (−Log10P)
Log2 Fold Change
Decrease excitability
Increase excitability
b
Disease association
Autism Spectrum Disorder
Epilepsy syndromes
Seizures
Schizophrenia
Frontotemporal Dementia
Alzheimer's Disease (late-onset)
Parkinson's Disease
c
r = 0.64
Screen replicate 2 gene score
Screen replicate 1 gene score

1502
1503

Extended Data Figure 3. Results from Primary screen

(a) Volcano plot summarizing the effect of knockdowns on CaMPARI phenotypes and the determine statistical significance for targeted genes (Mann-Whitney U test). Dashed lines indicate a false-discovery rate (FDR) cutoff of 0.05, based on the phenotype score for gene calculated from 5 targeting sgRNAs. Black points indicate hit genes where knockdown changes CaMPARI red/green fluorescence ratio in response to glutamate stimulation, while grey points indicate non-hits. Genes related to synaptic transmission (purple) and ion transport (orange) are highlighted based on Gene Ontology terms.

(b) Disease associated genes from DisGenNet and whole-exome sequencing (Satterstrom et al)9 overlap with hit genes from CaMPARI screen.

(c) Scatterplot of gene scores from each replicate of the primary screen shown the correlation between screens. Pearson's R = 0.49, linear regression fit depicted by solid black line.

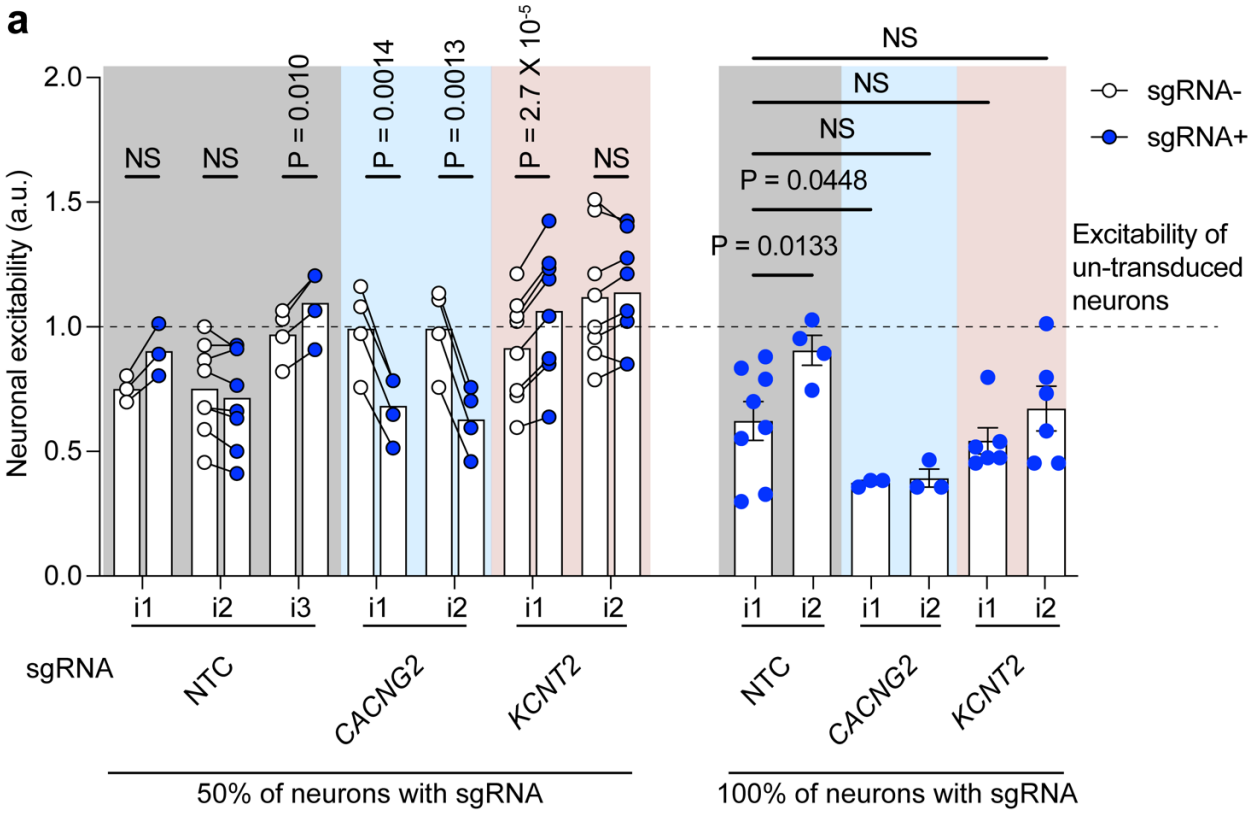
a
Neuronal excitability (a.u.)
2.0
1.5
1.0
0.5
0.0
NS
NS
P = 0.010
P = 0.0014
P = 0.0013
P = 2.7 X 10-5
NS
NS
NS
NS
P = 0.0448
P = 0.0133
sgRNA-
sgRNA+
Excitability of un-transduced neurons
i1
i2
i3
i1
i2
i1
i2
i1
i2
i1
i2
i1
i2
sgRNA
NTC
CACNG2
KCNT2
NTC
CACNG2
KCNT2
50% of neurons with sgRNA
100% of neurons with sgRNA

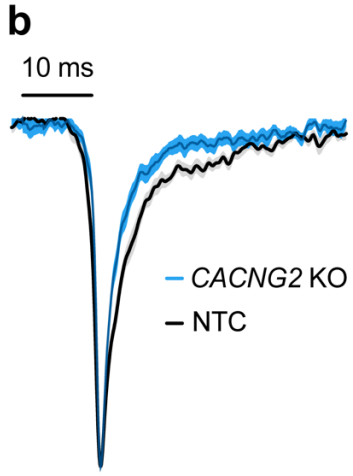
b
10 ms
CACNG2 KO
NTC

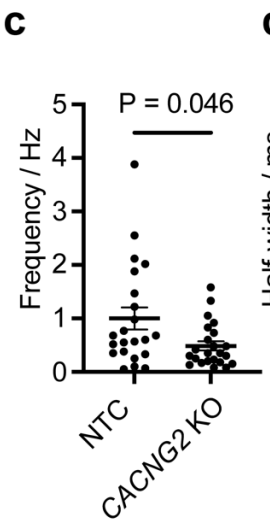
c
P = 0.046
Frequency / Hz
5
4
3
2
1
0
NTC
CACNG2 KO

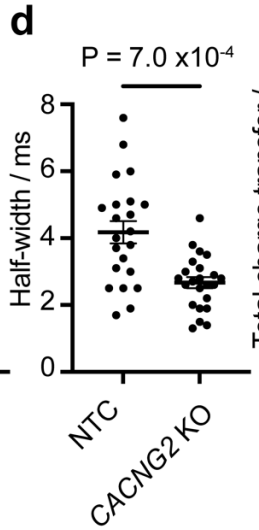
d
P = 7.0 x10-4
Half-width / ms
8
6
4
2
0
NTC
CACNG2 KO

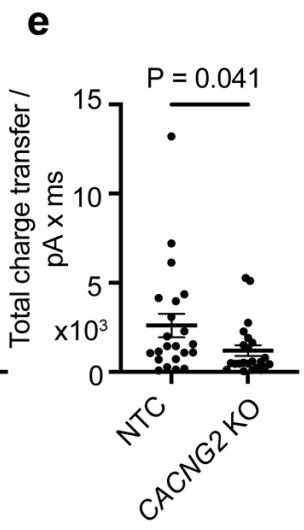
e
P = 0.041
Total charge transfer / pA x ms
x10³
15
10
5
0
NTC
CACNG2 KO

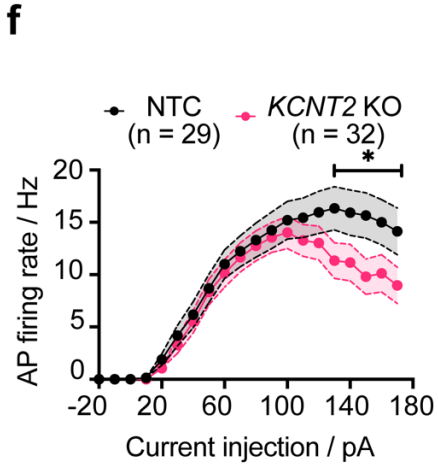
f
NTC (n = 29)
KCNT2 KO (n = 32)
*
AP firing rate / Hz
20
15
10
5
0
-20
20
60
100
140
180
Current injection / pA

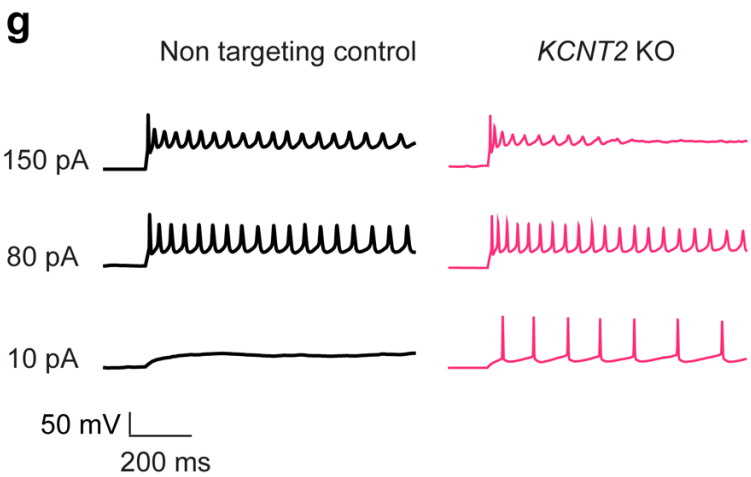
g
Non targeting control
KCNT2 KO
150 pA
80 pA
10 pA
50 mV
200 ms

Figure 3. CACNG2 and KCNT2 modify excitability in human neurons.

(a) CaMPARI2 neurons expressing sgRNAs targeting CACNG2 have reduced neuronal excitability in response to glutamate stimulation. This effect is observed intra-well, where CACNG2 sgRNA-containing neurons have a lower CaMPARI2 ratio than those that do not receive the sgRNA, and inter-well, in cultures in which 100% of the neurons are expressing the sgRNA. One of the sgRNAs targeting KCNT2 shows an increase in neuronal excitability when comparing intra-well effects, which matches the screening phenotype. In cultures where 100% of the neurons are expressing one of the sgRNAs targeting KCNT2, there is an unexpected decrease in the observed neuronal excitability. CaMPARI2 ratios are normalized to neuron samples that do not receive a sgRNA and are run on the flow cytometer on the same day. 50% knockdown cultures : N = 3-8 independent culture wells per experiment. Each individual experiment was normalized to the excitability (CaMPARI2 response) of wells where neurons did not receive a sgRNA. For intra-well comparisons, a paired ratio t-test between sgRNA- and sgRNA+ populations were performed for each sgRNA. The calculated P values are corrected for multiple hypothesis (Holm-Šídák method). For inter-well comparisons, P values were calculated by ANOVA, using NTC_i1 as reference. P > 0.05 = not significant (NS).

(b) The spontaneous excitatory postsynaptic currents (sEPSCs) in CACNG2 KO iNeurons demonstrate accelerated kinetics and a decrease in overall charge transfer. Averaged and normalized sEPSCs from all the recorded instances of NTCs (N = 22, in black) and CACNG2 KOs (N = 23, in blue), with the shaded area indicating standard errors.

(c) CACNG2 KOs exhibit reduced sEPSC frequency,

(d) half-width, and

(e) total charge transfer (Mann-Whitney test). NTCs (N = 22) and CACNG2 KOs (N = 23). Error bars denote standard error.

(f) KCNT2 KO neurons exhibit premature action potential failure. Current-spike output relationship presenting a diminished action potential firing rate in KCNT2 KOs (N = 32) at high current injection amplitudes, as juxtaposed against non-targeting controls (N = 29). The differences were statistically significant for current injection steps greater than 120 pA (asterisk donates p values as follows: 130 pA: p = 0.01, 140 pA : p = 0.02, 150 pA: p <0.01, 160 pA: p = 0.02, 170 pA: p = 0.01 ; two-way ANOVA with multiple comparisons).

(g) Sample recordings from both NTCs and KCNT2 KOs illustrating voltage responses of neurons to varying degrees of current injection.

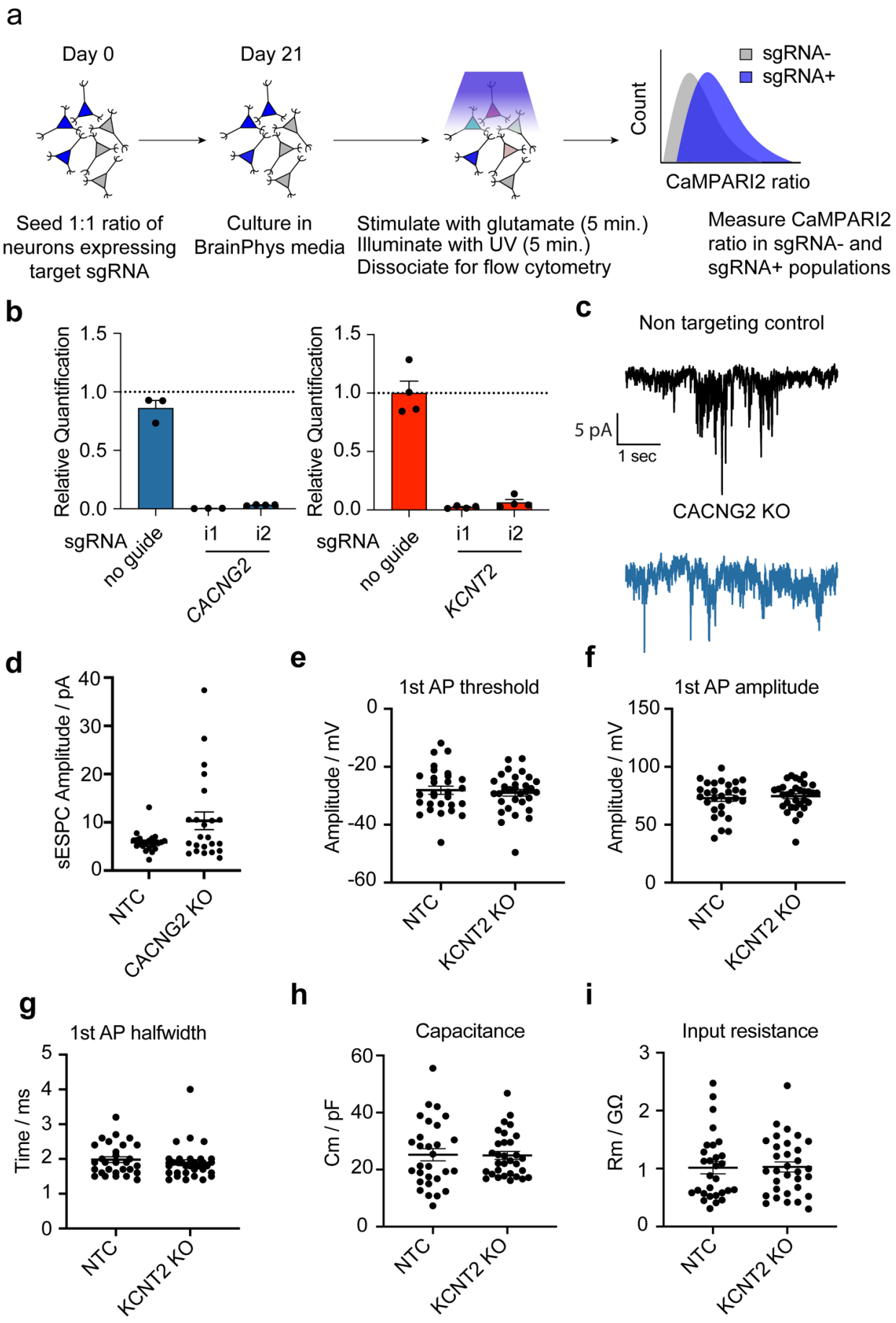
a
Day 0
Day 21
sgRNA-
sgRNA+
Count
CaMPARI2 ratio
Seed 1:1 ratio of neurons expressing target sgRNA
Culture in BrainPhys media
Stimulate with glutamate (5 min.)
Illuminate with UV (5 min.)
Dissociate for flow cytometry
Measure CaMPARI2 ratio in sgRNA- and sgRNA+ populations
b
Relative Quantification
sgRNA
no guide
i1
i2
CACNG2
KCNT2
c
Non targeting control
5 pA
1 sec
CACNG2 KO
d
sESPC Amplitude / pA
NTC
CACNG2 KO
e
1st AP threshold
Amplitude / mV
NTC
KCNT2 KO
f
1st AP amplitude
Amplitude / mV
NTC
KCNT2 KO
g
1st AP halfwidth
Time / ms
NTC
KCNT2 KO
h
Capacitance
Cm / pF
NTC
KCNT2 KO
i
Input resistance
Rm / GΩ
NTC
KCNT2 KO

Extended Data Figure 4. Electrophysiology profiles of iNeurons with KCNT2 and CACNG2 knockdowns.

(a) Schematic of intra-well comparison experiments with 50% of CaMPARI2 iNeurons expressing a sgRNA for a target gene. A 1:1 ratio of iNeurons expressing the sgRNA: not expressing a sgRNA are seeded and differentiated. These are then treated with the same glutamate and photoconversion conditions. These are gated based on the presence of BFP in the sgRNA construct, and the CaMPARI2 ratio is directly compared between the two populations.

(b) RT-qPCR shows the knock down efficiency of the sgRNAs targeting CACNG2 (blue) and KCNT2 (red). N = 4 biological replicates per condition. Error bars are SEM.

(c) Sample sEPSC recordings from NTC (black trace) and CACNG2 KO (blue trace) iNeurons

(d) CACNG2 KO iNeurons show a slight increase in sESPC amplitude that is not statistically significant. (NTC: 22 neurons, CACNG2 KO:23 neurons, Mann-Whitney test .

(e-i) No differences between NTCs (N= 29 neurons) and KNCT2 KOs (N = 32 neurons) in either passive membrane properties or action potential kinetics. Error bars donate standard error.

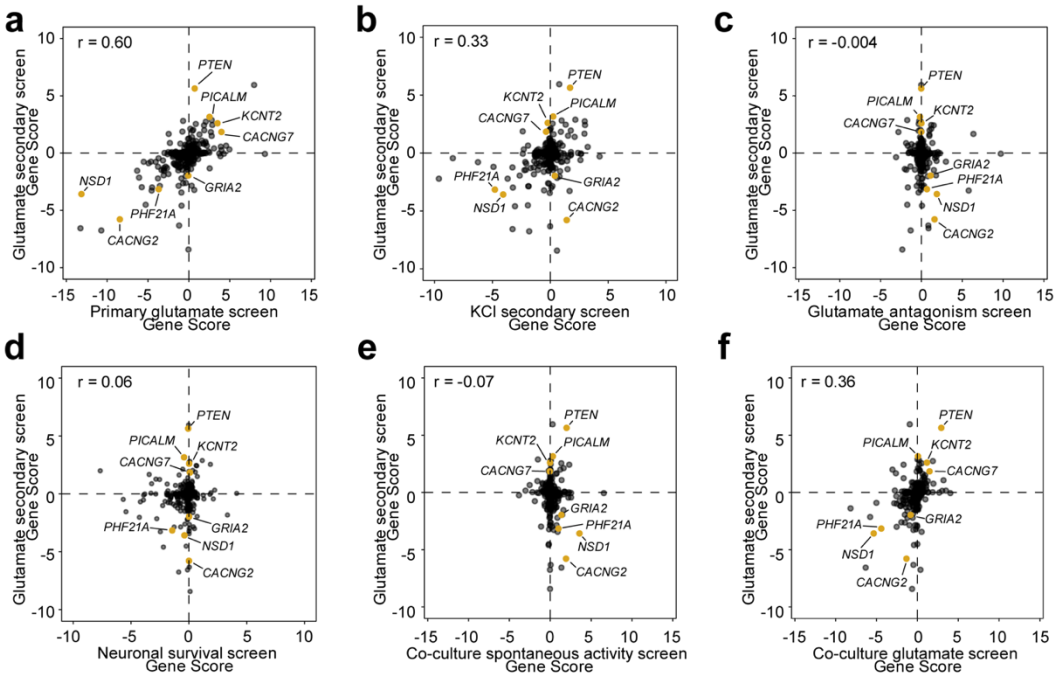
a
r = 0.60
PTEN
PICALM
KCNT2
CACNG7
NSD1
GRIA2
PHF21A
CACNG2
Glutamate secondary screen Gene Score
Primary glutamate screen Gene Score
b
r = 0.33
PTEN
KCNT2
PICALM
CACNG7
PHF21A
GRIA2
NSD1
CACNG2
Glutamate secondary screen Gene Score
KCl secondary screen Gene Score
c
r = -0.004
PTEN
PICALM
KCNT2
CACNG7
GRIA2
PHF21A
NSD1
CACNG2
Glutamate secondary screen Gene Score
Glutamate antagonism screen Gene Score
d
r = 0.06
PTEN
PICALM
KCNT2
CACNG7
PHF21A
GRIA2
NSD1
CACNG2
Glutamate secondary screen Gene Score
Neuronal survival screen Gene Score
e
r = -0.07
PTEN
KCNT2
PICALM
CACNG7
GRIA2
PHF21A
NSD1
CACNG2
Glutamate secondary screen Gene Score
Co-culture spontaneous activity screen Gene Score
f
r = 0.36
PTEN
PICALM
KCNT2
CACNG7
PHF21A
GRIA2
NSD1
CACNG2
Glutamate secondary screen Gene Score
Co-culture glutamate screen Gene Score

1575
1576

Figure 4. Secondary CRISPRi screens reveal excitability phenotypes in iPSC neurons.

(a) Comparison of gene scores across different screens. Gene scores of knockdowns in the primary and secondary screens with glutamate stimulation show a positive correlation (Pearson's R = 0.60).

(b) Many hit genes show similar phenotypes in neurons depolarized with KCl compared to those stimulated with glutamate (Pearson's R = 0.33).

(c) Glutamate receptor antagonists mostly abrogate phenotypes in neurons stimulated with glutamate, as reflected by a weak correlation of gene scores (Pearson's R = -0.004)

(d) Excitability phenotypes in glutamate-stimulated neurons are not strongly correlated with survival phenotypes (Pearson's R = 0.064).

(e) Modifiers of activity of spontaneously firing neurons in coculture do not correlate with those of glutamate-stimulated neurons in monoculture (Pearson's R = -0.07).

(f) Gene scores of knockdowns in the secondary screens with glutamate stimulation in monoculture and coculture show a positive correlation (Pearson's R = 0.36).

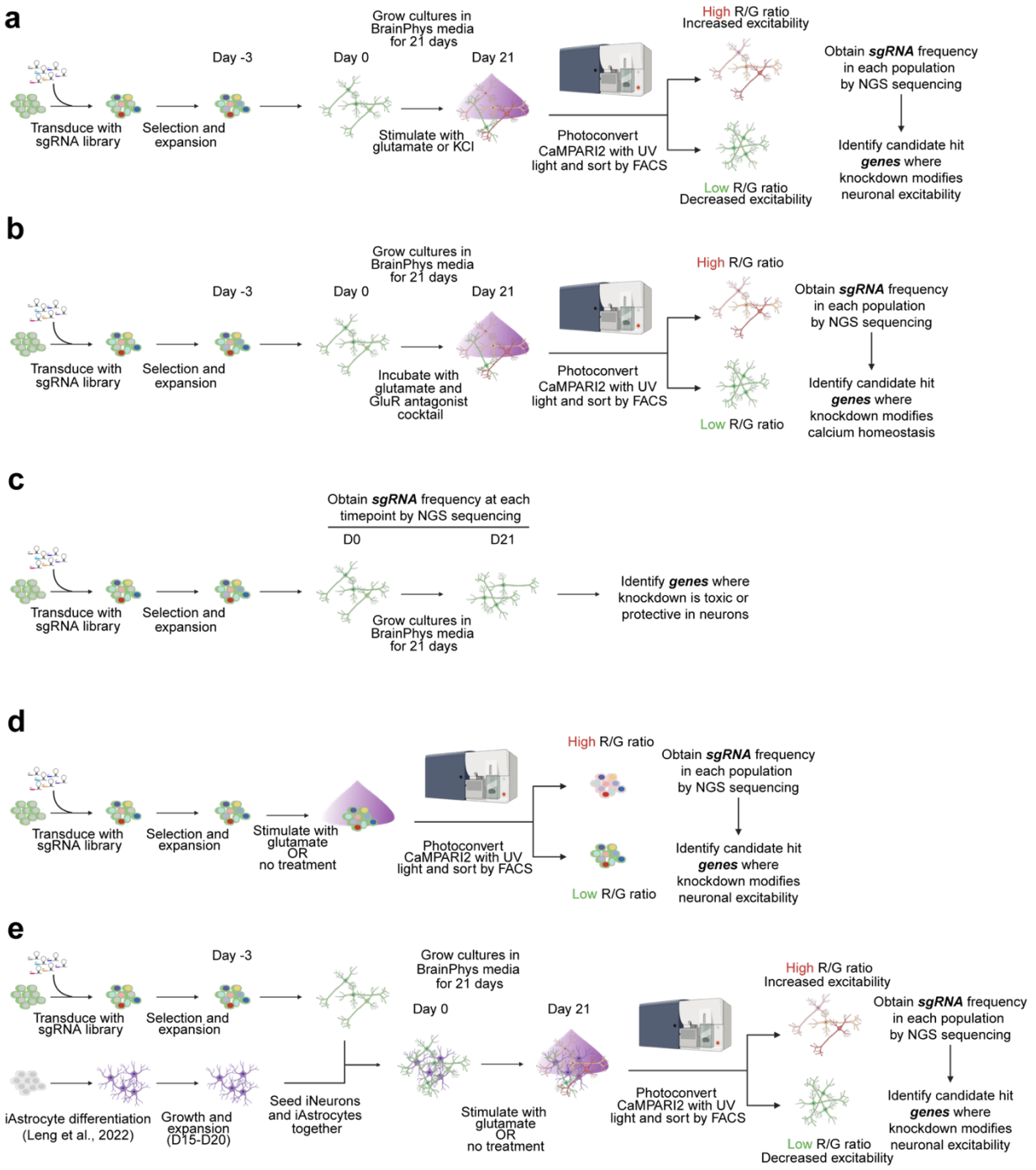

1596
1597
1598
1599

Extended Data Figure 5. Secondary CRISPRi screen strategies.

(a) Screening strategy. CRISPRi iPSCs were transduced with a pooled lentivirus sgRNA library consisting of hit genes from the primary screen (1622 sgRNAs targeting 424 genes). Exposure to puromycin selects for iPSCs successfully transduced with sgRNA construct. iPSCs were then differentiated into neurons via overexpression of NGN2 and cultured for 21 days. Neurons were then incubated with either 30 μM glutamate or 50 mM KCl, illuminated with UV light, and then separated by FACS into populations with high versus low red/green fluorescence ratios.

(b) iPSCs were differentiated into neurons via overexpression of NGN2 and cultured for 21 days. Neurons were then incubated with 30 μM glutamate, 1.5 μM TTX, 10 μM NBQX, 50 μM APV, 100 μM LY367385, 0.1 μM LY341495, 1 μM CPPG, 1 μM MTEP. Neurons were then illuminated with UV light, and then separated by FACS into populations with high versus low red/green fluorescence ratios.

(c) Survival of neurons was assessed by comparing sgRNA frequency in neurons at the start of differentiation (day 0) and after 21 days of differentiation.

(d) iPSCs expressing sgRNAs were treated with 30 μM glutamate for 5 minutes, illuminated with UV light, and then separated by FACS into populations with high versus low red/green fluorescence ratios.

(e) iPSCs expressing sgRNAs were differentiated into neurons and combined with Day 20 iAstrocytes. These co-cultures were grown for 21 days. Neurons were then treated 30 μM glutamate, illuminated with UV light, and then separated by FACS into populations with high versus low red/green fluorescence ratios. To assess the spontaneous activity of these cultures, no glutamate stimulation was applied.

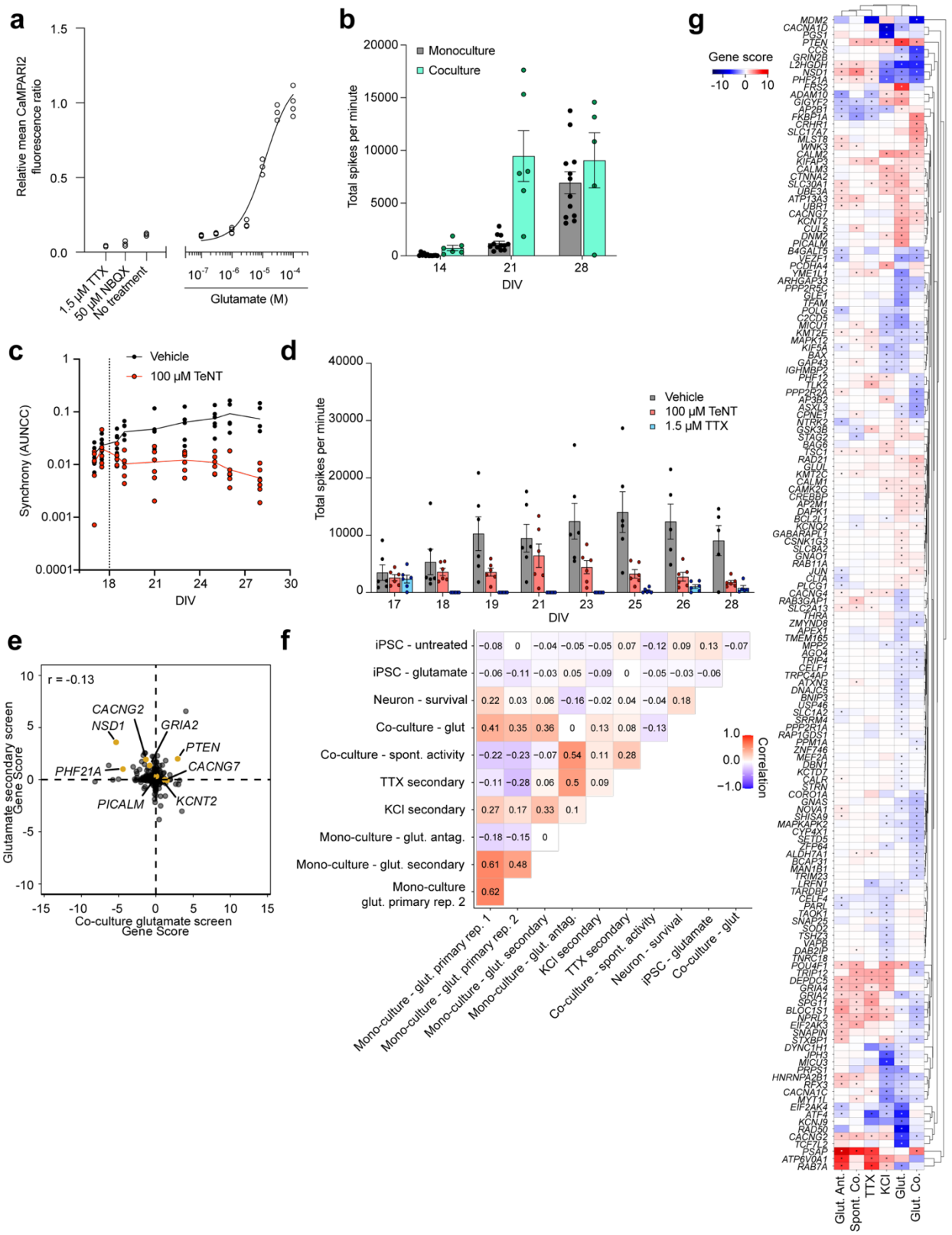

1625
1626
1627

Extended Data Figure 6. Secondary CRISPRi screens reveal excitability phenotypes in iPSC neurons.

(a) CaMPARI2 neurons in coculture with iAstrocytes respond to glutamate in a dose-dependent manner. N = 4 independent culture wells per measurement. TTX (1.5 μM), NBQX (50 μM), and “no treatment” conditions did not contain glutamate.

(b) Multielectrode arrays (MEA) recordings of spikes per minute of neuron-astrocyte cocultures and monoculture neurons. After 21 days of culture, more spikes are detected in cocultures. N = 6 independent culture wells, each with 16 electrodes.

(c) Synchrony of neuronal activity in neuron-astrocyte cocultures on MEA as measured through Area Under a Normalized Cross Correlation. After recording on day 18 (dotted line), cultures were treated with 100 μM tetanus toxin (TeNT) or vehicle control. Loss of synchrony begins around 24 hours later in TeNT treated wells, while vehicle treated wells show a slight increase. N = 6 independent culture wells, with 16 electrodes per well.

(d) Total spikes per minute of cultures from (c). Day 18 recording measured before addition of TeNT. N = 6 independent culture wells, with 16 electrodes per well.

(e) Modifiers of activity of spontaneously firing neurons in coculture do not correlate with those of glutamate-stimulated neurons in coculture (Pearson’s R = -0.13)

(f) Correlation matrix of gene scores from CaMPARI2 screens, using Pearson’s correlation.

(g) Heatmap of gene scores in secondary screens. Each included gene is classified as a hit in at either the KCl or glutamate (monoculture and coculture) screens (FDR > 0.1) and is denoted with an asterisk when classified as a hit.

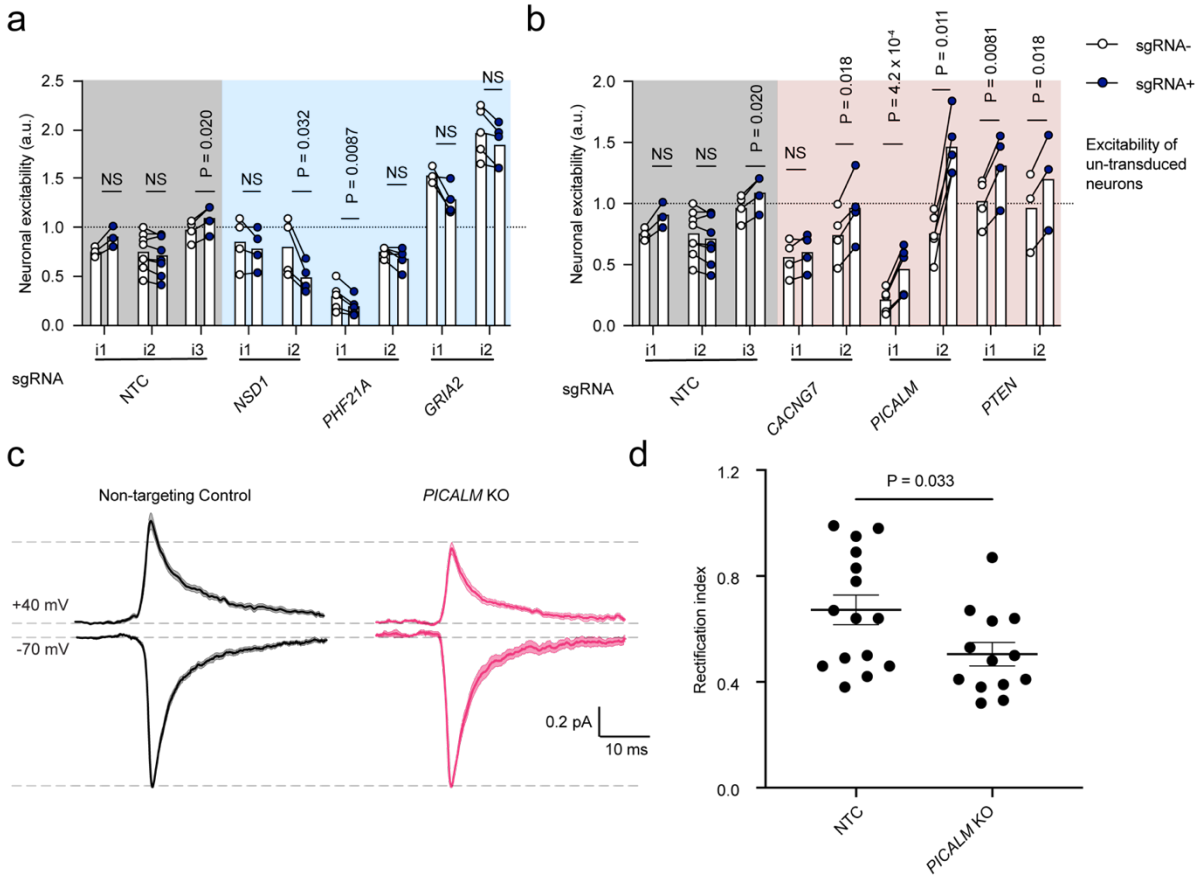

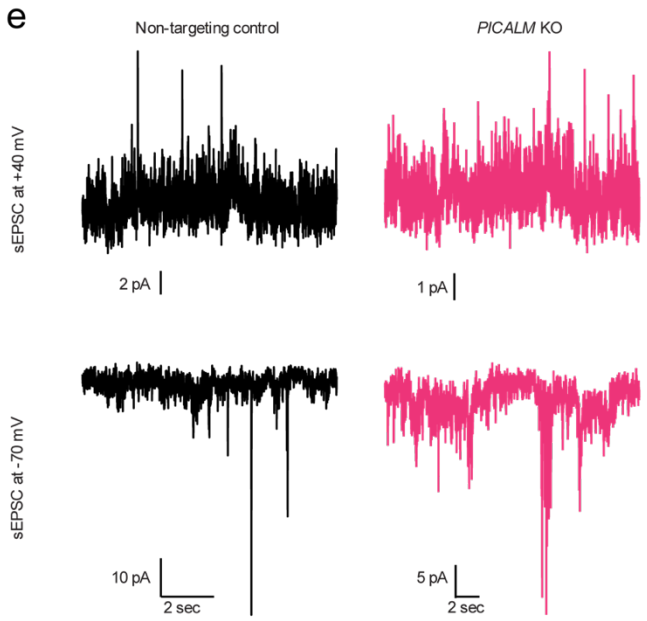

1654
1655
1656
1657

Figure 5. Flow validation of disease-associated excitability hit genes.

(a) CaMPARI2 neurons expressing sgRNAs targeting genes that, when knocked down, reduced neuronal excitability in response to glutamate stimulation in the secondary screens. This effect is observed intra-well, where sgRNA-containing neurons have a lower CaMPARI2 ratio than those that did not receive a sgRNA. Non-targeting controls (NTCs) are the same as in Figure 3A. Paired ratio t-test made between neuron populations receiving sgRNA (sgRNA+) and not receiving guide (sgRNA-). N = 3-6 independent culture wells per measurement. Each individual experiment was normalized to the excitability (CaMPARI2 response) of wells where neurons did not receive a sgRNA. For intra-well comparisons, a paired ratio t-test between sgRNA- and sgRNA+ populations were performed for each sgRNA. The calculated P values were corrected for multiple hypotheses (Holm-Šídák method).

(b) CaMPARI2 neurons expressing sgRNAs targeting genes that, when knocked down, increased neuronal excitability in response to glutamate stimulation in the secondary screens. This effect is observed intra-well, where sgRNA containing neurons have a higher CaMPARI2 ratio than those that do not receive a sgRNA. Non-targeting controls (NTCs) are the same as in Figure 3A and Figure 5A . Paired ratio t-test made between neuron populations receiving sgRNA (sgRNA+) and not receiving guide (sgRNA-). N = 3-6 independent culture wells per measurement. Each individual experiment was normalized to the excitability (CaMPARI2 response) of wells where neurons did not receive a sgRNA. For intra-well comparisons, a paired ratio t-test between sgRNA- and sgRNA+ populations were performed for each sgRNA. The calculated P values were corrected for multiple hypotheses (Holm-Šídák method).

(c) PICALM KOs exhibit a reduced rectification index (the ratio of current magnitude at +40 mV vs -70 mV) relative to NTC, suggesting an increased presence of synaptic calcium permeable AMPA receptors. The traces represent the mean and standard error of all sEPSC recordings from NTC and PICALM KO iNeurons and are shown normalized to the average -70 mV sEPSC for each neuron. (N = 15 NTC, 13 PICALM KO).

(d) PICALM KOs displayed a decreased rectification index as compared to NTCs (N = 15 and 13 neurons for NTCs and PICALM KOs, respectively; analyzed using the Mann-Whitney test). Error bars donate standard error.

(e) Sample sEPSC recordings from representative NTC and PICALM KO iNeurons.

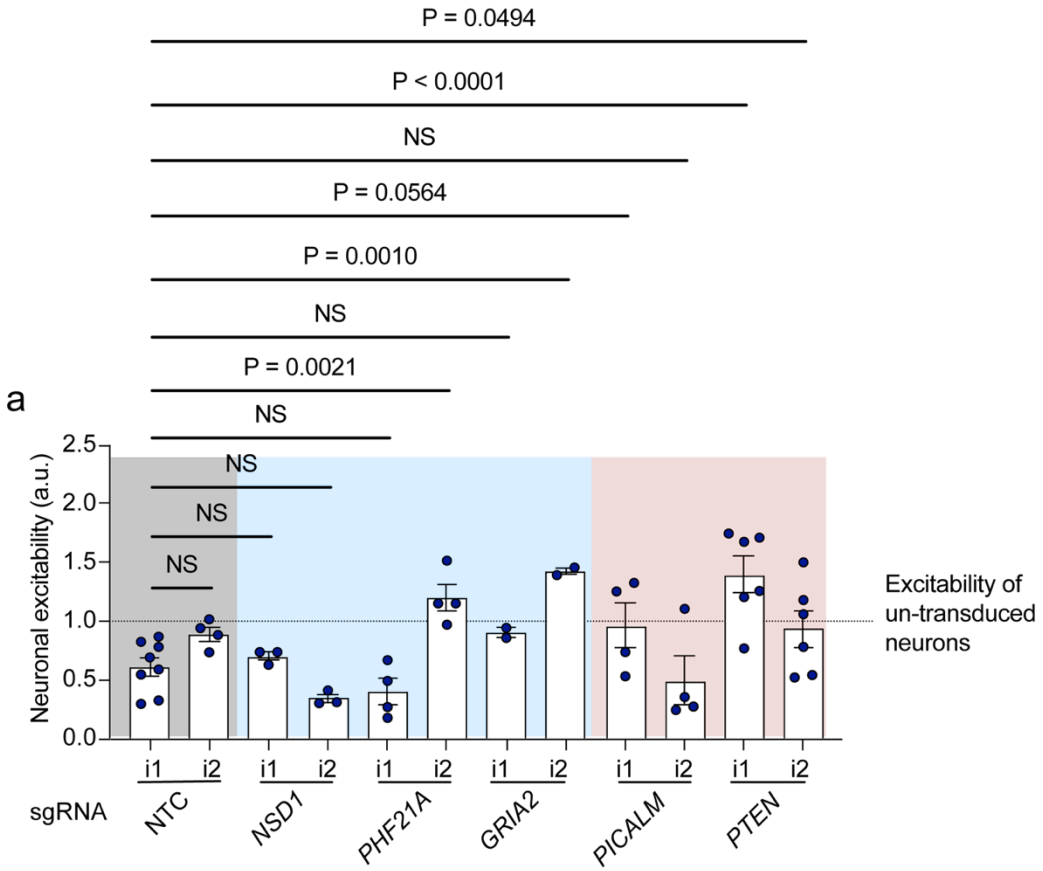

Extended Data Figure 7. Validation of KDs from secondary screens

In cultures where 100% of CaMPARI2 iNeurons are expressing sgRNAs targeting NSD1 and PHF21A, these iNeurons lack statistically significant reduced neuronal excitability in response to glutamate stimulation observed in the screen relative to non-targeting controls. iNeurons expressing sgRNAs targeting PTEN show the expected increase in activity. For iNeurons expressing sgRNAs targeting GRIA2 and PICALM, the expected screen phenotype is not preserved when 100% of the cells have the knockdown. CaMPARI2 ratios are normalized to neuron samples that do not receive a sgRNA and are run on the flow cytometer on the same day. N = 2-8 independent culture wells per experiment. Each individual experiment was normalized to the excitability (CaMPARI2 response) of wells where neurons did not receive a sgRNA. Error bars denote standard error. P values calculated by ANOVA, using NTC_i1 as reference. P > 0.05 = not significant (NS).

1709

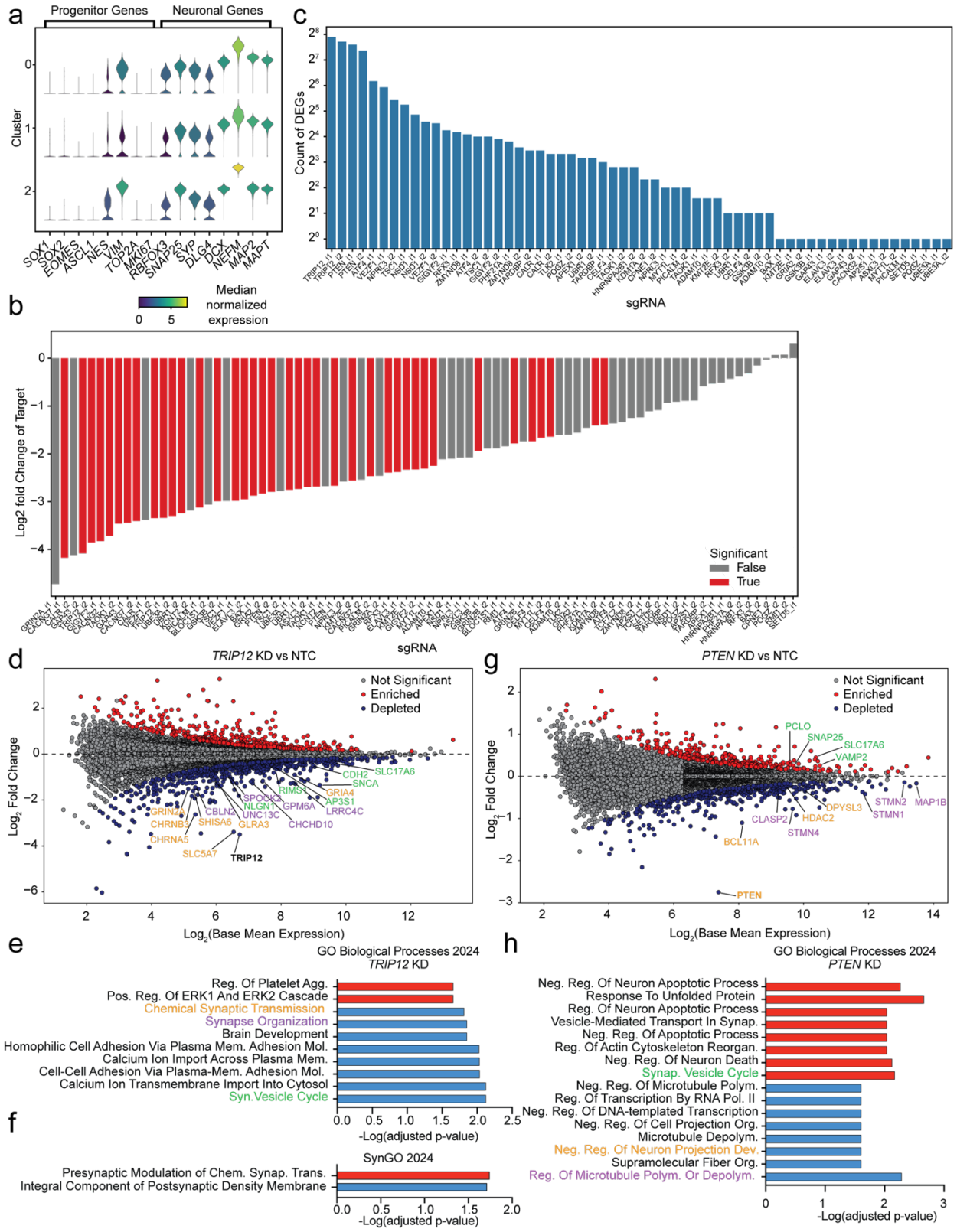

1710
1711

Figure 6. CROP-seq reveals transcriptional changes to genes involved in synaptic processes drive changes in excitability.

(a) Marker gene expression is homogenous across clusters and suggests that neuronal identity is conserved.

(b) On-target knockdown of target genes and the corresponding sgRNAs. Red bars indicated a significant KD in comparison to NTCs, while grey bars did not reach significance.

(c) Number of significantly differentially expressed genes for each detected sgRNA. Each sgRNA was compared separately to the group of five non-targeting control (NTC) sgRNAs, and significance was determined at a threshold of and adjusted p-value <0.05.

(d) MA plot of TRIP12 knockdown, showing genes (colors indicate associated GO term in Figure 6e) related to synaptic transmission and synapse organization.

(e) GO term (Biological Processes) enrichment analysis of upregulated (red) and downregulated genes in TRIP12 KD

(f) GO term (SynGO) enrichment analysis of upregulated (red) and downregulated genes in TRIP12

(g) MA plot of PTEN knockdown, showing an upregulation of synaptic processes and downregulation of microtubule organization and polymerization. Genes are colored ti indicate associated GO term in Figure 6h.

(h) GO term (Biological Processes) enrichment analysis of upregulated (red) and downregulated genes in PTEN KD.

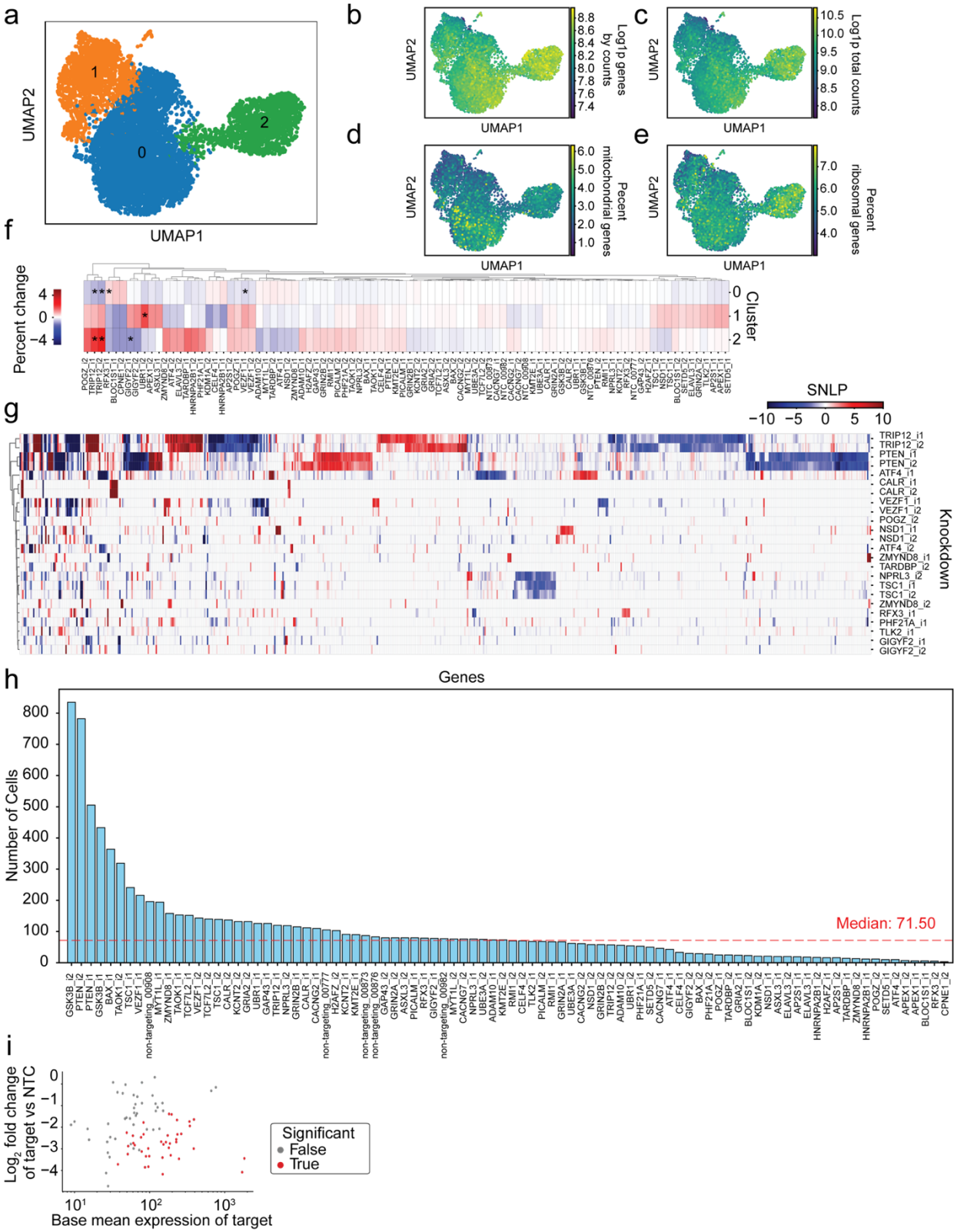
a
UMAP2
UMAP1
0
1
2
b
Log1p genes by counts
c
Log1p total counts
d
Pecent mitochondrial genes
e
Percent ribosomal genes
f
Percent change
Cluster
g
SNLP
Knockdown
h
Genes
Number of Cells
Median: 71.50
i
Log2 fold change of target vs NTC
Base mean expression of target
Significant
False
True

Extended Data Figure 8. CROP-seq reveals transcriptional changes to genes involved in synaptic processes drive changes in excitability.

(a) Leiden clustering of neurons from CROP-seq classified into 3 clusters.

(b) Log(1+P) genes detected in each cell.

(c) Log(1+P) total read counts in each cell.

(d) Percentage of mitochondrial genes detected in each cell.

(e) Percentage of ribosomal genes detected in each cell.

(f) Heatmap of cluster shift analysis for each knockdown. Color values are expressed as the percent change in abundance of the knockdown in each cluster relative to non-targeting controls. Asterisks denote significant enrichments and depletions (adjusted q-value < 0.05).

(g) Heatmap of differentially expressed genes (DEGs, versus non-targeting controls, adjusted p-value < 0.05) of knockdowns with significant on-target KD. Clustering shows consistency between individual sgRNAs targeting the same gene. SNLP is signed negative log of the adjusted p-value. Knockdowns with >10 DEGs are shown.

(h) sgRNA representation by number of neurons detected in scRNA-seq data post quality control filtering and with a sgRNA MOI of one.

(i) Plot of on-target KD versus base mean expression for each sgRNA. Lower expression of genes generally resulted less ability to call significance.